https://doi.org/10.5194/gmd-2020-85
Preprint. Discussion started: 2 June 2020

Geoscientific Model Development Discussions

Integrated Modeling of Photosynthesis and Transfer of Energy, Mass and Momentum in the Soil-Plant-Atmosphere Continuum System

Yunfei Wang[a, b, c], Yijian Zeng[c], Lianyu Yu[c], Peiqi Yang[c], Christiaan Van de Tol[c], Huanjie Cai[a, b, ※], Zhongbo Su[c, d, ※],

[a] College of Water Resources and Architectural Engineering, Northwest Agriculture and Forestry University, Yangling, China
[b] Institute of Water Saving Agriculture in Arid Regions of China (IWSA), Northwest Agriculture and Forestry University, Yangling, China
[c] Faculty of Geo-Information Science and Earth Observation, University of Twente, Enschede, the Netherlands
[d] Key Laboratory of Subsurface Hydrology and Ecological Effect in Arid Region of Ministry of Education, School of Water and Environment, Chang'an University, Xi'an, China

※ Correspondence: Huanjie Cai (huanjiec@yahoo.com); Zhongbo Su (z.su@utwente.nl)

Abstract. Root water uptake is an important component of the terrestrial water balance and a critical factor that influences energy, water vapor, and carbon exchange among soil, vegetation and atmosphere interfaces. However, most of the current vegetation photosynthesis models do not account for root water uptake, which compromises their applications under water stressed conditions. To address this limitation, this study integrates photosynthesis and transfer of energy, mass and momentum in the soil-plant-atmosphere continuum system, via a simplified 1D root growth model and a resistance scheme (from soil, through root zones and plants, to atmosphere). The coupled model was evaluated with field measurement of a maize canopy. The results indicated that the simulation of land surface fluxes was significantly improved due to considering the root water uptake, especially when vegetation is experiencing severe water stress. This finding highlights the importance of enhanced soil heat and moisture transfer, as well as dynamic root distribution, on simulating ecosystem functioning.

Key words: SCOPE model; STEMMUS model; Soil-Plant-Atmosphere Continuum (SPAC) system; Root Water Uptake (RWU); Root system growth

1. Introduction

Root water uptake (RWU) by plants is a critical process controlling water and energy exchanges between the land surface and the atmosphere, as well as the plant growth. The representation of RWU is an essential component of eco-hydrological models that simulate terrestrial water, energy and carbon fluxes (Seneviratne et. al., 2010; Wang and Smith, 2004). However, most of these models consider the above-ground processes in much greater detail than below-ground processes, and therefore, they have limited ability represent the dynamic response of plant water uptake to water stress. Compensatory Root

https://doi.org/10.5194/gmd-2020-85
Preprint. Discussion started: 2 June 2020


Geoscientific Model Development Discussions

Water Uptake (CRWU) refers to the process by which uptake from sparsely rooted but well-watered parts of the root zone compensates for stress in other parts (Jarvis, 2011). The failure to account for compensatory water uptake and the associated hydraulic lift from deep subsoil (Caldwell et al., 1998; Dawson, 1993) can lead to significant uncertainties in simulating the plant growth and corresponding eco-hydrological processes (Desborough, 1997; Lee et al., 2005; Seneviratne et. al., 2010; Teuling et al., 2006; Zeng and Dai, 1998).

Furthermore, the macroscopic RWU model needs to calculate Hydraulic Redistribution (HR) (Caldwell et al., 1998; Espeleta et al., 2004; Amenu and Kumar, 2007; Fu et al. 2016) (Table 1). Ideally, a RWU model is based on the soil-plant-atmophere continuum concept (SPAC-RWU), and considers the redistribution of soil water with compensatory water uptake as well as the flow of water from soil through the plant to the atmosphere (Guo, 1992).

The spatial (i.e., one dimensional vertical) pattern of RWU is determined by the spatial distribution of the root system, the knowledge of which is essential for predicting the spatial distribution of water contents and water fluxes in soils. The distribution of roots and their growth are sensitive to various physical, chemical, and biological factors, as well as to soil hydraulic properties that influence the availability of water and oxygen for plants (Beaudoin et al., 2009). Many attempts have been made in the past to develop root growth models that account for the influence of various environmental factors such as temperature, aeration, soil water availability, and soil compaction. Existing root growth models ranged from complex, three-dimensional root architecture models (Bingham and Wu, 2011; Leitner et al., 2010; Wu et al., 2005) to much simpler root growth models that are implemented within more complex models such as EPIC (Williams et al., 1989) and DSSAT (Robertson et al., 1993). Most of these models reproduce the measured rooting depth very well, but the distribution of new growth root is based on empirical functions rather than biophysical processes (Camargo and Kemanian, 2016) (Table 1).

Modelling RWU requries representation of above and below ground processes, which is realized via SPAC-RWU. The SPAC-RWU model represents a good compromise between simplicity (i.e., a small number of tuning parameters) and the ability to capture non-linear responses of RWU (and subsequently the ecosystem functioning) to drought events. Specifically, the SPAC-RWU model calculates the CRWU term using the gradient between leaf water potential and soil water potential of each soil layer. The HR process is an extreme case of CRWU occurring when the transpiration is relatively small and the RWU terms in some soil layers are negative due to leaf water potential was higher than soil water potential. The most important parameters in the SPAC-RWU model include the leaf water potential, stomatal resistance, and the root resistance. Different from other macroscopic models using the root distribution function, the SPAC-RWU model needs explicitly the root length density at each soil layer to calculate the root resistance for each soil layer (Deng et al. 2017). The most practical method for obtaining the root length density is using the root growth model.

To understand the ecosystem functioning under drought stress, the sub-models for below and above ground are therefore needed to be coupled via the afore-mentioned resistance schemes, which control the flow of water from soil to root, root to

https://doi.org/10.5194/gmd-2020-85
Preprint. Discussion started: 2 June 2020


Geoscientific Model Development Discussions

plant and plant to atmosphere. Furthermore, the coupling should be realized also via the interface: one sub-model provides the boundary conditions for the other. The below-ground process model simulates the Simultaneous Transfer of Energy, Momentum, and Mass in Unsaturated Soil (i.e., STEMMUS model), the running of which requires land surface energy fluxes and land surface temperature. On the other hand, the required surface boundary state and fluxes can be provided with the above-ground process model, for example, the vegetation photosynthesis model, SCOPE (Soil Canopy Observation, Photochemistry, and Energy Fluxes).

The SCOPE model simulates canopy reflectance and fluorescence spectra in the observation directions, as well as photosynthesis, and evapotranspiration as functions of leaf optical properties, canopy structure, and weather variables (Van der Tol et al. 2009). SCOPE model provides a valuable means to study the link between vegetation appearance and ecosystem functioning, however, it does not consider the water budget in soil and vegetation. As such, there is no explicit parametrization of the effects of soil moisture variations on the photosynthetic or stomatal parameters. Consequently, soil moisture effects are only 'visible' in SCOPE model if the lack of soil moisture affects the optical or thermal appearance of the vegetation (i.e., during water stress period). The lack of such link between soil moisture availability and vegetation appearance compromises the capacity of SCOPE for predicting/simulating drought events.

The change of vegetation optical appearance as a result of soil moisture variations can only explain partially the soil moisture effect on ecosystem functioning (Bayat et al., 2018), which leads to considerably biased estimations of *GPP* (Gross Primary Productivity) and *ET* (Evapotranspiration) in water limited conditions. This presents a challenge for using SCOPE for ecosystems in arid and semi-arid areas, where water availability is the primary limiting factor for vegetation functioning. This challenge becomes even more relevant considering that soil moisture deficit or "ecological drought" is expected to increase in both frequency and severity at nearly all ecosystems around the world (Zhou et al., 2013). Bayat et al. (2019) incorporated the SPAC model into SCOPE to address water stress conditions at a grassland site, but the coupled model neglected the dynamic development of root distribution at different soil layers and soil moisture serves only as a model input coming from measurements.

In this study, the modelling of above-ground radiation, energy fluxes in the vegetation layer (i.e., SCOPE) will be fully coupled with the soil heat and mass transfer model - STEMMUS (Simultaneous Transfer of Energy, Mass and Momentum in Unsaturated Soil). The root growth model and the corresponding resistance scheme (from soil, through root zones and plants, to atmosphere) will be integrated for the dynamic modeling of water stress and root system, enabling the seamless modelling of soil-water-plant-energy interactions. The next *section of methodology* describes the coupling scheme between SCOPE and STEMMUS models, followed by the *section of results* verifying the coupled SCOPE_STEMMUS model at a maize agroecosystem located in a semi-arid region. The *discussion session* explores and reveals the dynamic responses of leaf water potential and root length density to water stress. The summary of this study and the further challenges are addressed in the *section of conclusions*.

https://doi.org/10.5194/gmd-2020-85
Preprint. Discussion started: 2 June 2020

Geoscientific Model Development Discussions
Open Access
EGU

Table 1. Comparison of LSMs and crop models in terms of sink term calculation of soil water balance.

	Model	Sink term calculation of soil water balance	Root water uptake process		
			Hydraulic redistribution (Richards and Caldwell, 1987)	Compensatory uptake (Jarvis, 2011)	Root fraction
LSMs	CLM4.5	Actual transpiration, root fraction of each soil layer and soil integral soil water availability (Fu et al., 2016)	The Ryel et al. (2002) Function	Not considered	Empirical function
	CLM4.0	Actual transpiration, root fraction of each soil layer and soil integral soil water availability (Couvreur et al. 2012, Sulis et al., 2019)	HRWU scheme (RWU model based on hydraulic architecture)	HRWU scheme	Empirical function
	CLM3 & IBIS2	Actual transpiration, physical root distribution and the water availability in each layer (Zheng and Wang, 2007)	The Ryel et al. (2002) Function	Dynamic root water uptake	Empirical function
	CoLM	Total transpiration, root fraction in each layer and water stress factor (Zhu et al., 2017)	The Ryel et al. (2002) Function and the Amenu and Kumar (2007) function	Empirical approach with a compensatory factor	Empirical function
	CABLE	Maximal efficiency of water uptake by roots and available soil water (Li et al., 2012)	The Ryel et al. (2002) Function	Not considered	Empirical function
Crop Models	APSIM	Potential transpiration and water supply factor, but neglect root distribution (Keating et al., 2003)	Not considered	Not considered	Empirical function
	CropSyst	Difference in water potential between the soil and the leaf, and a total soil–root–shoot conductance (Stöckle et al., 2003)	Not considered	Considered by the leaf and soil water potential	Linear decrease in soils with no limitations to root exploration
	DSSAT	Water uptake per unit of root length is computed as an exponential function, and the actual RWU is the minimum of potential transpiration and the maximum capacity of root water uptake (Jones et al., 2003)	Not considered	Water uptake per unit of root length as a function of soil moisture	Using an empirical function
	EPIC	EPIC assumes that water is used preferentially from the top layers, and the potential water supply rate decreases exponentially downward. (Williams et al.,2014)	Not considered	Not considered	Not considered
	SWAP	Based on the potential transpiration, root fraction and an empiric stress factor relationship (van Dam, 2000)	Not considered	Based on soil water potential	Function of relative rooting depth
	WOFOST	The simplest one, it calculates water uptake as a function of the rooting depth and the water available in that rooting depth without regard to the soil water distribution with depth (Supit et al., 1994)	Not considered	Not considered	Empirical function
	SPACSYS	According to empirical root length density distribution in a soil layer, potential transpiration and soil moisture (Wu et al., 2005)	Not considered	Not considered	1D (empirical function) or 3D root system (process based)
	STICS	Based on the potential transpiration, root fraction, and soil water distribution, but not process based (Beaudoin et al., 2009)	Not considered	Not considered	1D root length density profile

https://doi.org/10.5194/gmd-2020-85
Preprint. Discussion started: 2 June 2020


Geoscientific Model Development Discussions

2. Methodology and Data

2.1. SCOPE and SCOPE_SM Models

SCOPE is a radiative transfer and energy balance model (Van der Tol et al. 2009). It simulates the transfer of optical, thermal and fluorescent radiation of the vegetation canopy and computes *ET* by using an energy balance routine. SCOPE includes a radiative transfer module for incident solar and sky radiation to calculate the top of canopy outgoing radiation spectrum, net radiation and absorbed photosynthetically active radiation (*aPAR*), a radiative transfer module for thermal radiation generated internally by soil and vegetation to calculate the top of canopy outgoing thermal radiation and net radiation, an energy balance module for latent heat, sensible heat and soil heat flux, and a radiative module for chlorophyll fluorescence to calculate the top of canopy radiance spectrum of fluorescence at leaf level.

Compared to other radiative transfer models which simplify the radiative transfer processes based on Beer's Law, SCOPE has well-developed radiative transfer modules which consider the various leaf orientation and the multiple scattering. SCOPE can provide detailed information about net radiation of every leaf within the canopy. Furthermore, SCOPE is based on energy balance and it can simulate soil surface temperature which is a vital boundary condition needed by STEMMUS. In addition, Bayat et al. (2019) developed SCOPE_SM, which was based on SCOPE but considering the effect of soil moisture (as model inputs). Therefore, SCOPE_SM provides the basic framework to couple SCOPE with STEMMUS, however both SCOPE and SCOPE_SM ignored the soil heat and mass transfer processes and the dynamics of root growth. Appendix A.1 lists the main equations of calculating water stress factor within SCOPE (Bayat et al. 2019), the detailed formulation of SCOPE is referred to Van der Tol et al. (2009).

2.2. STEMMUS Model

STEMMUS model is a two-phase mass and heat transfer model with explicit consideration of the coupled liquid, vapor, dry air and heat transfer in unsaturated soil (Zeng et al. 2011a,b; Zeng and Su, 2013; Yu et al. 2018). STEMMUS provides a comprehensive description of water and heat transfer in the unsaturated soil, which can compensate what is currently neglected in SCOPE. The boundary condition needed by STEMMUS includes surface soil temperature, which is the output of SCOPE. In addition, STEMMUS already contained an empirical equation to calculate root water uptake and a simplified root growth module to calculate root fraction profile. As such, STEMMUS has an ideal model structure to be coupled with SCOPE. The main governing equations of STEMMUS are listed in Appendix A.2.

2.3 Dynamic Root Growth and Root Water Uptake

To obtain the root resistance of each soil layer, we incorporated a root growth module to simulate the root length density profile (see Appendix A.3). The simulation of root growth refers to the root growth module in the INRA STICS crop growth

https://doi.org/10.5194/gmd-2020-85
Preprint. Discussion started: 2 June 2020


Geoscientific Model Development Discussions

model (Beaudoin et al., 2009), which includes the calculations of root front growth and root length growth. The root front growth is a function of temperature, with the depth of the root front beginning at the sowing depth for sown crops and at an initial value of transplanted crops or perennial crops (Beaudoin et al., 2009). The root length growth is calculated in each soil layer, considering the net assimilation rate and the allocation fraction of net assimilation on root, which is subsequently a function of LAI (leaf area index) and root zone water content (Krinner et al. 2005). The root length density profile is then used to calculate the root resistance to water flow radially across the roots, soil hydraulic resistance, and plant axial resistance to flow from the soil to the leaves (see Appendix A4).

2.4 SCOPE_STEMMUS Coupling

The coupling starts with an initial soil moisture (*SM*) profile simulated by STEMMUS, which enables the calculation of the water stress factor, a reduction factor of the maximum carboxylation rate (V_{cmax}), SCOPE is then used calculate net photosynthesis (*An*) or gross primary productivity (*GPP*), soil respiration (*Re*), energy fluxes (*Rn*, *LE*, *H* and *G*), transpiration (*T*), which is passed to STEMMUS as the root water uptake (RWU). Then, the net ecosystem exchange (*NEE*) can be calculated based on *An* and *Re*. Surface soil moisture is also used in calculating soil surface resistance and then calculating soil evaporation (*E*). Furthermore, SCOPE can calculate soil surface temperature (T_{s0}) based on energy balance, which was subsequently used as the top boundary condition of STEMMUS. Based on RWU, STEMMUS calculates the soil moisture in each layer at the end of the time step, and the new soil moisture profile will be the soil moisture at the beginning of next time step, which is repeated as such till the end of simulation period. The time-step of SCOPE_STEMMUS is flexible and the time step used in this study was half hour. Figure 1 shows the coupling scheme of STEMMUS and SCOPE, and Table B.1 shows all the parameter values used in this study.

https://doi.org/10.5194/gmd-2020-85
Preprint. Discussion started: 2 June 2020

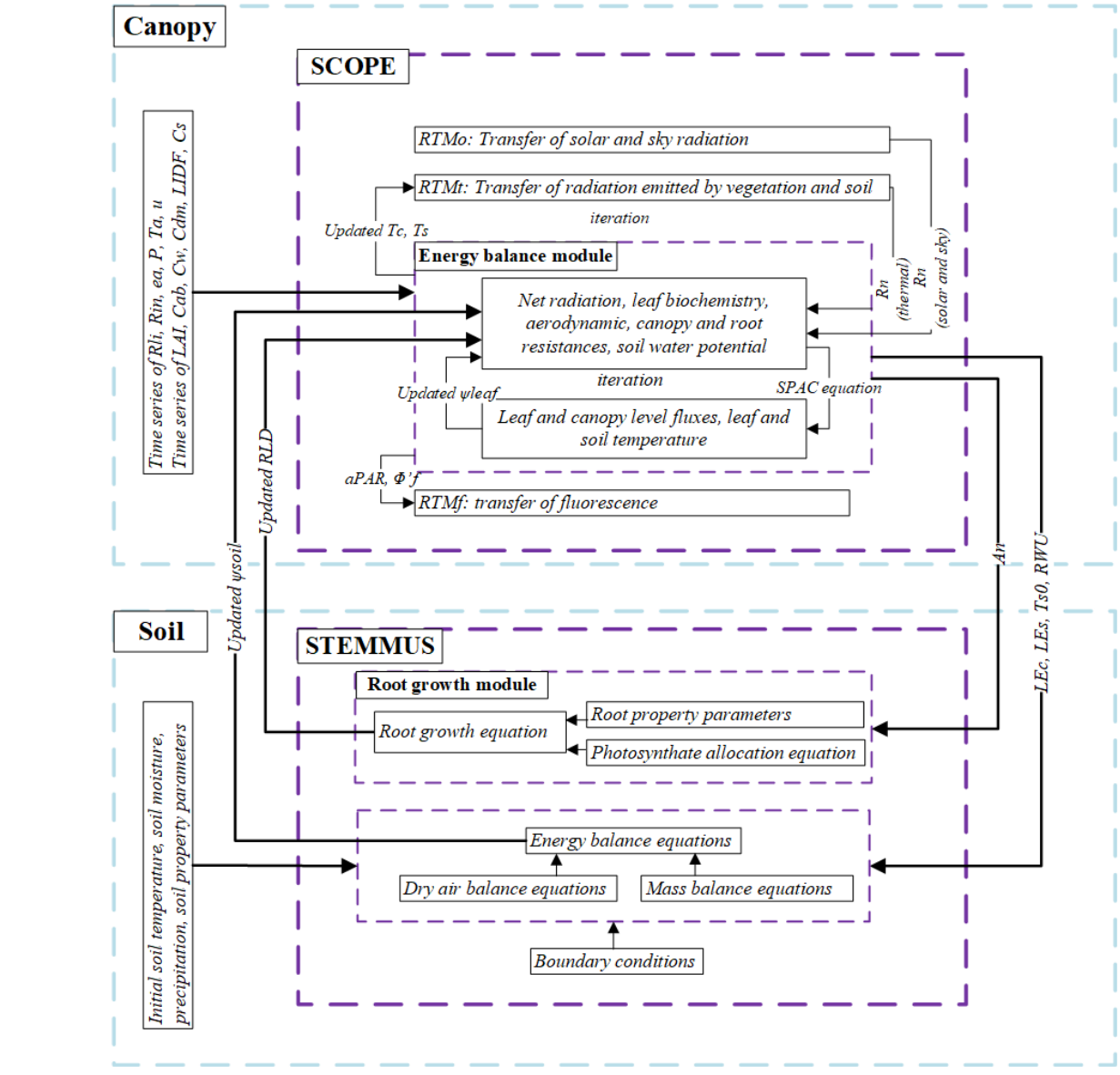

Figure 1. The coupling scheme of SCOPE_STEMMUS (Yu et al. (2018), Van der Tol et al. (2009)). The explanations of the symbols were the same as in Table B.1.

https://doi.org/10.5194/gmd-2020-85
Preprint. Discussion started: 2 June 2020


Geoscientific Model Development Discussions

2.5. Evapotranspiration partitioning

Most studies in partitioning evapotranspiration (*ET*) use sap flow and micro lysimeter data from in-situ measurements. In this study, we used a simple and practical method to separate evaporation (*E*) and transpiration (*T*) proposed by Zhou et al. (2016). Although the behavior of plant stomata is influenced by environmental factors, the potential water use efficiency ($uWUE_p$, g C $hPa^{0.5}$/kg H_2O) at stomatal scale in the ecosystem with a homogeneous underlying surface is assumed to be nearly constant (Medlyn et al., 2011), and variations of actual *uWUE* (g C $hPa^{0.5}$/kg H_2O) can be attributed to the soil evaporation (Zhou et al., 2016). Thus, the method can be used to estimate *T* and E with the quantities of *ET*, *uWUE* and $uWUE_p$. Another assumption of this method is that the ecosystem *T* equal to *ET* at some growth stages, so $uWUE_p$ can be estimated using the upper bound of the ratio of $GPP\sqrt{VPD}$ to *ET* (here *GPP* refers to Gross Primary Productivity, and VPD to Vapor Pressure Deficit) (Zhou et al., 2014; Zhou et al., 2016).

Zhou et al. (2016) used the 95th quantile regression between $GPP\sqrt{VPD}$ and *ET* to estimate $uWUE_p$, and showed that the 95th quantile regression for $uWUE_p$ at flux tower sites was consistent with the *uWUE* derived at the leaf scale for different ecosystems. In addition, the variability of seasonal and interannual $uWUE_p$ was relatively small for a homogeneous canopy. Therefore, the calculations of $uWUE_p$, *uWUE*, and *T* at the ecosystem scale were as follows:

$$uWUE_p = \frac{GPP\sqrt{VPD}}{T} \quad (1)$$

$$uWUE = \frac{GPP\sqrt{VPD}}{ET} \quad (2)$$

$$\frac{T}{ET} = \frac{uWUE}{uWUE_p} \quad (3)$$

The calculation of *VPD* was based on air temperature and relative humidity data, and the method of gap-filling was the Marginal Distribution Sampling *(MDS)* method proposed by Reichstein et al. (2005). To calculate *GPP*, the complete series of net ecosystem exchange *(NEE)* was partitioned into gross primary production *(GPP)* and respiration *(Re)* using the method proposed by Reichstein et al. (2005). Finally, *ET* was calculated using the latent heat flux and air temperature. Based on *GPP*, *ET* and *VPD* data, *T* can be calculated using the method proposed by Zhou et al. (2016).

Meanwhile, Zhou et al. (2016) discussed the uncertainty of this method, which was mainly caused by: (1) the uncertainty in the partitioning of *GPP* (less than 10%) and *Re* based on *NEE*, which would result in some uncertainty in *uWUE*; (2) due to the seasonal variation of atmosphere CO_2 concentration, the assumption of $uWUE_p$ being constant would cause some uncertainty (less than 3%); (3) the assumption of *T* being equal to *ET* sometimes during the growing season would cause some uncertainty when vegetation is sparse.

https://doi.org/10.5194/gmd-2020-85
Preprint. Discussion started: 2 June 2020


Geoscientific Model Development Discussions

2.6. Field measurements

To evaluate the performance of SCOPE_STEMMUS in modeling ecohydrological processes, simulation was conducted to compare SCOPE_STEMMUS with SCOPE, SCOPE_SM, and STEMMUS using the observation of fluxes (from 10 June 2017 to 10 October) at the Yangling station (34°17′ N, 108°04′ E, 521 m a.s.l.). Figure 2 illustrates the variations of environmental factors during the maize growing season. As shown in the subfigures, the incoming shortwave radiation ranged from 0 to 1100 W m^{-2} and decreased significantly after Days-After-Sowing (hereafter as DAS) 67. In contrast, the incoming longwave radiation was relatively stable, which was about 400 W m^{-2} during the maize season. The air temperature was relatively high at initial stage and gradually decreased to 5 ^{o}C at the late stage. The soil moisture was maintained at a high level except during a drought episode from DAS 15 to 40, and the relative humidity (*RH*) at the late stage was higher than that at the early stage. Two irrigations were carried out on DAS 7 and DAS 41, and the volume of irrigation were 28mm and 64mm, respectively. The leaf area index (LAI) and canopy height (hc) were measured and the peak value was 4.39 m^2 m^{-2} and 1.95 m, respectively. Due to the lack of field measurement on root length and soil moisture profile of root zone, we used the simulated results of SCOPE_STEMMUS as the input data of SCOPE_SM to compare the performance of SCOPE_SM with that of SCOPE_STEMMUS. The Eddy Covariance (EC) system was installed on a height-adjustable tripod, The EC system included a three-dimensional sonic anemometer, an open path infrared gas analyser, and a data logger. The detailed descriptions of the instruments can refer to Wang et al. (2020).

https://doi.org/10.5194/gmd-2020-85
Preprint. Discussion started: 2 June 2020

Geoscientific Model Development
Discussions
Open Access
EGU

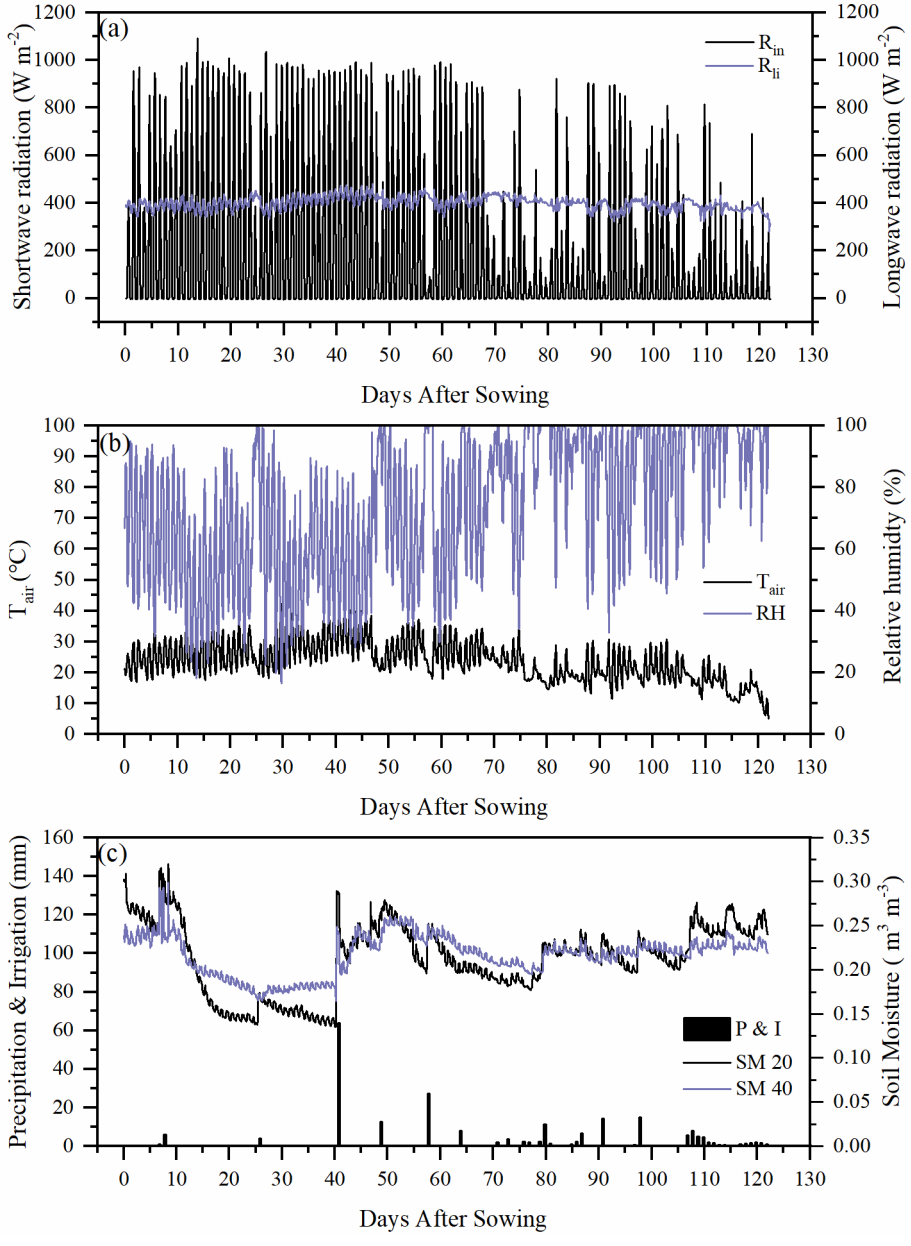

190

https://doi.org/10.5194/gmd-2020-85
Preprint. Discussion started: 2 June 2020

Geoscientific Model Development Discussions

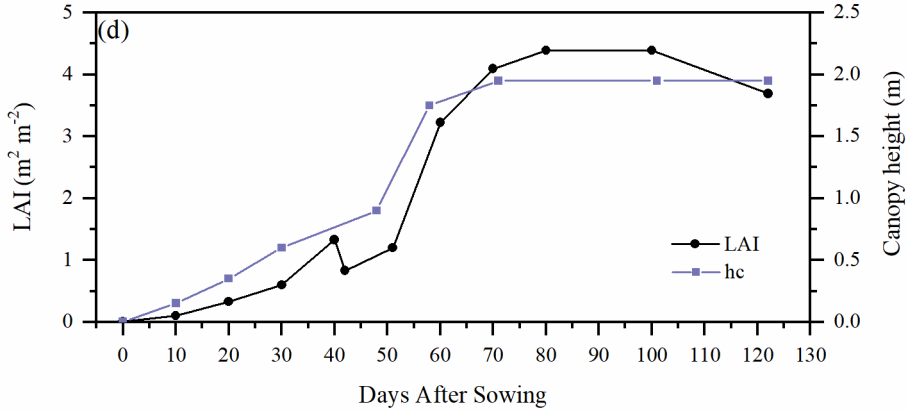

Figure 2 Seasonal variation of environmental factors for maize growing season at Yangling, China. (a) incoming shortwave radiation (R_{in}) and incoming longwave radiation (R_{li}) (b) air temperature (T_{air}) and relative humidity (RH); (c) volumetric soil water content at 20, and 40 cm depths (SM 20, and SM 40) and daily precipitation/irrigation (P&I); (d) leaf aera index (LAI) and canopy height (hc)

2.7. Performance Metrics

The metrics used to evaluate the performance of coupled SCOPE_STEMMUS model include: (1) Root Mean Squared Error (*RMSE*); (2) coefficient of determination (R^2); and (3) the index of agreement (*d*). They are calculated as:

$$RMSE = \sqrt{\frac{1}{n}\sum_{i=1}^{n}(P_i - O_i)^2} \quad (4)$$

$$R^2 = \frac{\left[\sum_{i=1}^{n}(P_i-\bar{P})(O_i-\bar{O})\right]^2}{|\bar{O}|} \quad (5)$$

$$d = 1 - \frac{\sum_{i=1}^{n}(P_i-O_i)^2}{\sum_{i=1}^{n}(|P_i-\bar{O}|+|O_i-\bar{O}|)^2} \quad (6)$$

where P_i is the *i*th predicted value, O_i is the *i*th observed value, $\bar{O}$ is the average of observed values, and *n* is the number of samples.

3. Results

3.1. Soil moisture modeling

Comparison of simulated soil moisture (*SM*) using STEMMUS and SCOPE_STEMMUS and observed ones is presented in Figure 3. The simulated soil moisture at 20 cm depth agreed with the observed values in terms of seasonal pattern. Although slight overestimation occurred at initial and late stages, the dynamics in soil moisture resulted from precipitation or irrigation were well captured. Per the nature of the two models, the coupling of SCOPE with STEMMUS is not expected to improve

https://doi.org/10.5194/gmd-2020-85
Preprint. Discussion started: 2 June 2020

the simulation of soil moisture. However, compared to SCOPE_SM, which used soil moisture measurements as inputs, the coupled SCOPE_STEMMUS improves the simulation of soil moisture dynamics as measured. The deviation between the model simulations and the measurements can be attributed to the following two potential reasons. First, the field observation has errors to a certain extent and the soil moisture sensors may be not well calibrated. Second, in this simulation, we assumed that the soil texture was homogeneous in the vertical direction, whereas the soil properties (e.g. soil bulk density and saturated hydraulic conductivity) may vary with depth in reality, and at different growth stages due to field management practices. For example, the soil bulk density at 40 cm was much higher than that at 20 cm due to the mechanical tillage, especially in the early stage.

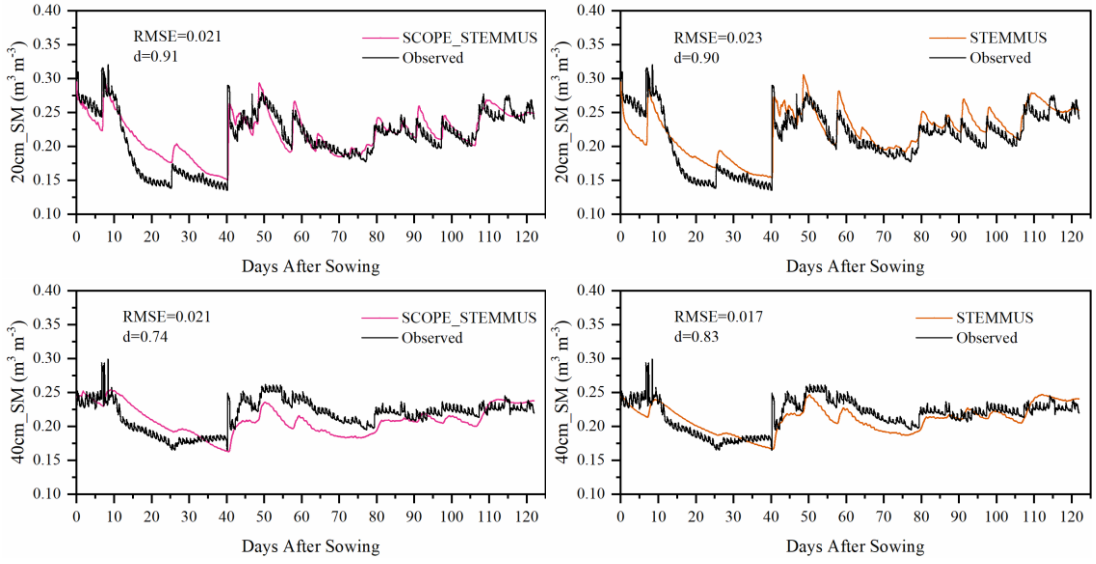

Figure 3 Comparison of observed and modeled soil moisture at 20 cm (20 cm_SM) and 40 cm depth (40 cm_SM)

3.2. Soil temperature modeling

Simulated soil temperatures (*Ts*) by STEMMUS and SCOPE_STEMMUS at 20 cm and 40 cm depth are shown in Figure 4. In general, both two models can capture the dynamic of soil temperature well. For the simulation of 20 cm temperature, for STEMMUS and SCOPE_STEMMUS, RMSE value was 2.56 ºC and 2.58 ºC, respectively; d value was 0.92 and 0.92, respectively. For the simulation of 40cm temperature, RMSE value was 2.06 ºC and 2.07 ºC, respectively; d value was 0.93 and 0.93, respectively. These results indicate that both models can simulate well soil temperature. However, there also exist some differences between simulation and observation. The largest difference occurred in DAS 40, when the field was irrigated with the flooding irrigation method. This irrigation activity may lead to the boundary condition errors (i.e., for soil surface temperature), which cannot be estimated well enough (e.g., there is no monitoring of water temperature from the irrigation). Meanwhile, the measurement may also have some errors in this period. The fact for the observed soil temperature

https://doi.org/10.5194/gmd-2020-85
Preprint. Discussion started: 2 June 2020

Geoscientific Model Development Discussions

at 20 cm and 40 cm to decrease to almost the same level at the same time indicates a potential pathway for preferential flow in the field (see precipitation/irrigation at DAS 40 in Figure 2), and the sensors captured this phenomenon. Nevertheless, the model captures the soil temperature dynamics.

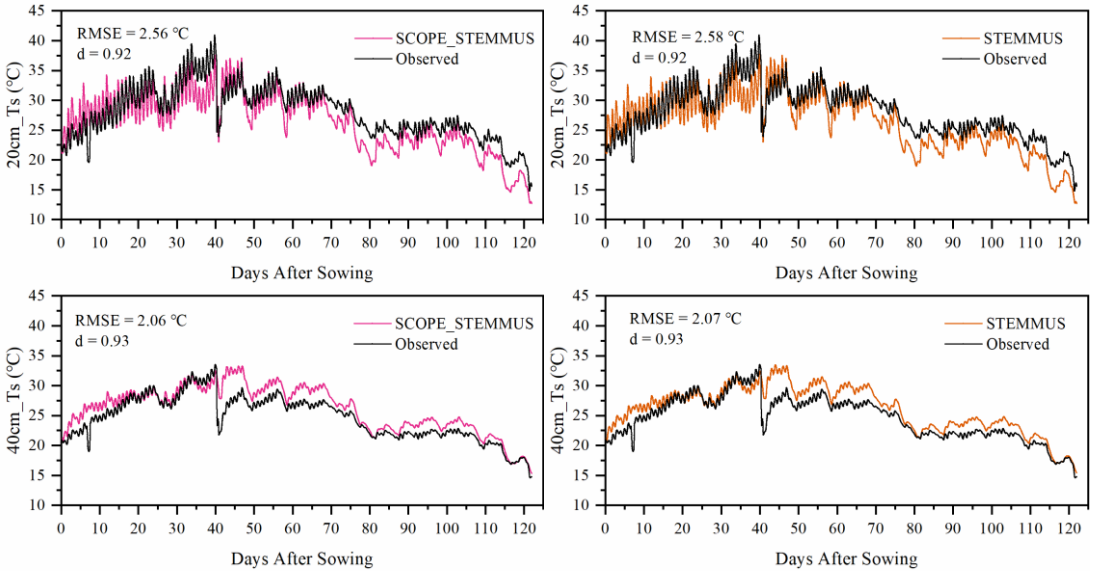

Figure 4 Comparison of observed and modeled soil temperature at 20 cm (20 cm_Ts) and 40 cm depth (40 cm_Ts).

3.3. Energy balance modeling

A comparison of the observed and modeled half-hourly net radiation (*Rn*), sensible heat flux (*H*), latent heat flux (*LE*), and soil heat flux (*G*) using original SCOPE, SCOPE_SM, and SCOPE_STEMMUS were presented in Figure 5. For net radiation and soil heat flux, the simulations of all three models show good agreements with observations. For net radiation, the coefficients of determination (R^2) for SCOPE, SCOPE_SM and SCOPE_STEMMUS were 0.99, 1.00, and 0.99, respectively. For soil heat flux, the R^2 for SCOPE, SCOPE_SM and SCOPE_STEMMUS were 0.81, 0.79, and 0.80, respectively. For latent heat flux, SCOPE_STEMMUS has a better performance than SCOPE and SCOPE_SM, and the R^2 for SCOPE, SCOPE_SM and SCOPE_STEMMUS were 0.82, 0.84, and 0.85, respectively. Furthermore, SCOPE_STEMMUS and SCOPE_SM have a similar performance in the simulation of sensible heat flux, which were better than the performance of SCOPE, the R^2 for SCOPE, SCOPE_SM and SCOPE_STEMMUS were 0.70, 0.75, and 0.74, respectively.

https://doi.org/10.5194/gmd-2020-85
Preprint. Discussion started: 2 June 2020

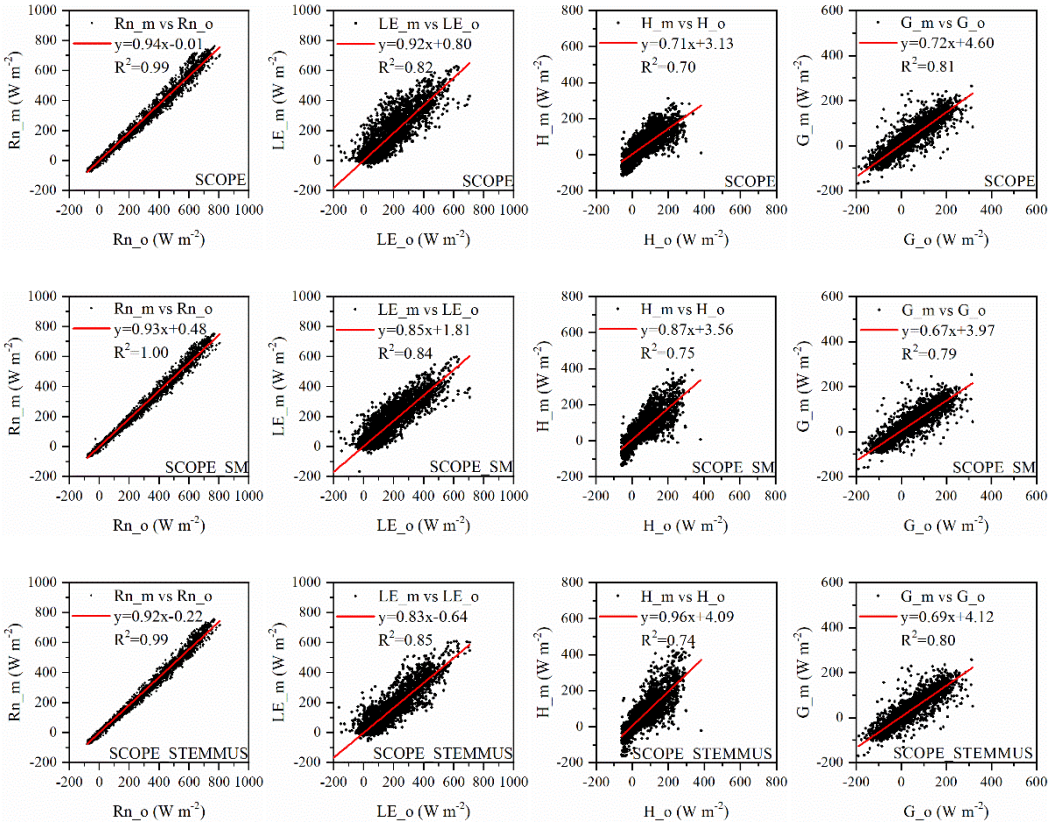

Figure 5 Comparison of observed and modeled half-hourly Net radiation (Rn), Latent heat (LE), Sensible heat (H) and soil heat flux (G) by SCOPE, SCOPE_SM and SCOPE_STEMMUS. Subscripts '_m' and '_o' in each plot indicate modeled and observed quantities, respectively. The regression line is indicated in red color with the corresponding regression equation and the R^2.

3.4. Daily ET, T and E modeling

Simulated daily evapotranspiration (ET) results by SCOPE, SCOPE_SM, STEMMUS and SCOPE_STEMMUS are presented in Figure 6. As shown in the subfigures, the R^2 by SCOPE, SCOPE_SM, STEMMUS and SCOPE_STEMMUS were 0.76, 0.82, 0.80 and 0.81, respectively. The *RMSE* of these four models were 0.84, 0.69, 0.76, and 0.74 mm day^{-1} respectively. For the ET simulation by SCOPE, there were large differences between simulations and observations when the vegetation suffered water stress. For SCOPE_SM, STEMMUS and SCOPE_STEMMUS, because of taking into account the dynamic variation of soil moisture, the simulated ET were closer to observations when the crop experienced water stress. It indicates that SCOPE_STEMMUS, STEMMUS and SCOPE_SM can predict ET with a relatively higher accuracy, especially when the maize was under severe water stress (DAS 30 to 40), and SCOPE_STEMMUS and SCOPE_SM performed similarly well. It is noteworthy that although STEMMUS has considered the effect of soil moisture on ET, the accuracy of STEMMUS was lower than the coupled model (see DAS 40 and DAS 110 in Figure 6). The possible reason is

https://doi.org/10.5194/gmd-2020-85
Preprint. Discussion started: 2 June 2020

Geoscientific Model Development Discussions

the better representation of transpiration in SCOPE model (see Figure 7), which separates the canopy into 60 layers, while STEMMUS only treats the canopy as one layer.

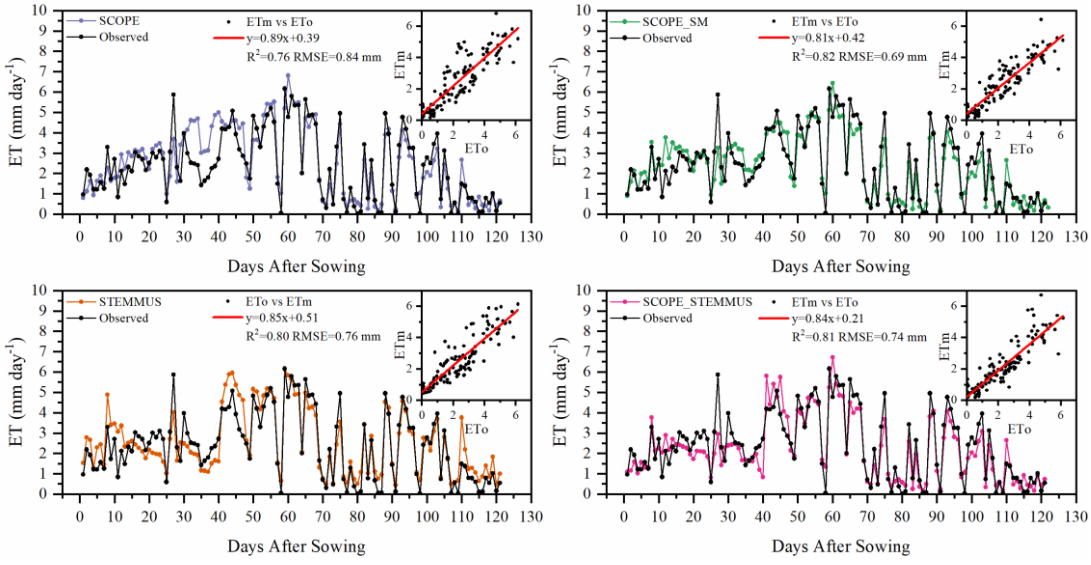

Figure 6 Comparison of modeled and observed daily evapotranspiration (ET) (ETo: observed ET; ETm: modeled ET).

The modeled and observed daily plant transpiration are presented in Figure 7. The R^2 value between simulated and observed transpiration were 0.82, 0.86, 0.79, and 0.86, respectively, for SCOPE, SCOPE_SM, STEMMUS and SCOPE_STEMMUS, and *RMSE* values were 0.60, 0.50, 0.67, and 0.50 mm day^{-1}, respectively. Because of ignoring the effect of water stress on transpiration, SCOPE failed to simulate transpiration accurately when the vegetation experiencing water stress. As shown in the figure, SCOPE overestimated transpiration from DAS 20 to DAS40 during the water stress period. Compared with SCOPE, SCOPE_SM, STEMMUS and SCOPE_STEMMUS can capture the reduction of transpiration during the dry period. The performances of SCOPE_STEMMUS and SCOPE_SM were better than that of STEMMUS. The possible reason is the better simulation of the radiative transfer and energy balance at leaf level in the coupled SCOPE_STEMMUS model (as also in SCOPE_SM) and the more accurate root water uptake (compared to that in SCOPE_SM). Nevertheless, SCOPE_STEMMUS slightly underestimated transpiration when the plant is undergoing severe water stress and slightly overestimated it after the crop was irrigated. This is mainly because the actual V_{cmax} was not only influenced by drought but also related to leaf nitrogen content (Xu and Baldocchi, 2003), which was not considered in this study.

https://doi.org/10.5194/gmd-2020-85
Preprint. Discussion started: 2 June 2020

Geoscientific Model Development Discussions

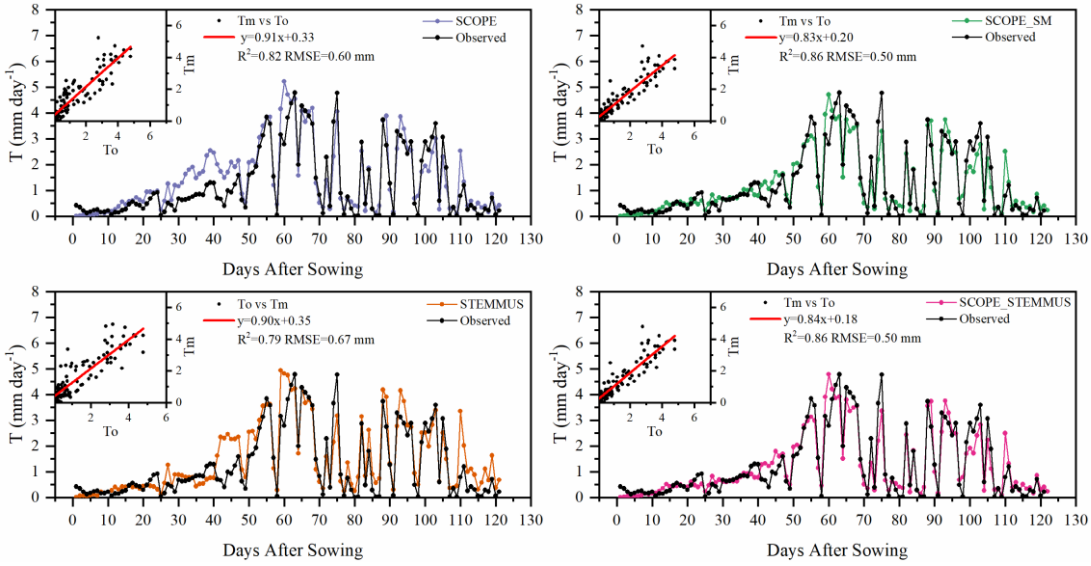

Figure 7 Comparison of observed and modeled daily plant transpiration (T) (To: observed T; Tm: modeled T).

Figure 8 shows the modeled and observed half-hourly canopy transpiration. The simulations by SCOPE_STEMMUS and SCOPE_SM are consistent with observation and both are much lower than that by SCOPE. The performances of SCOPE_STEMMUS and SCOPE_SM were consistent with that of SCOPE in the early morning and late afternoon, when the photosynthesis is mainly limited by incident radiation rather than by water stress, intercellular CO_2 concentration and V_{cmax}. In the midday, with increasing incident radiation, the photosynthesis was mainly limited by water stress and V_{cmax}, exactly when the simulations by SCOPE_STEMMUS and SCOPE_SM are much better than that by SCOPE.

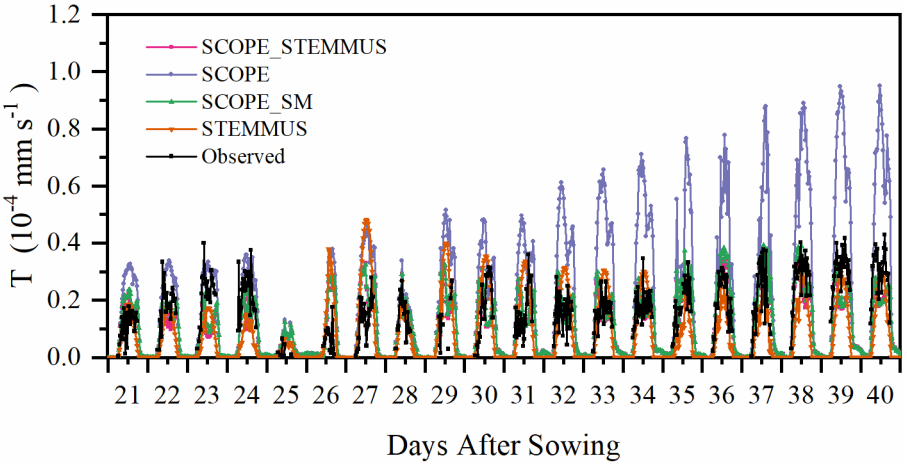

Figure 8 Comparison of observed and modeled half-hourly transpiration (T).

https://doi.org/10.5194/gmd-2020-85
Preprint. Discussion started: 2 June 2020

Geoscientific Model Development Discussions

As shown in Figure 9 for soil evaporation, the simulation by SCOPE_STEMMUS is closer to observation than those by other models. When using SCOPE to simulate soil evaporation, the soil moisture is set as constant (i.e., 0.25 m^3 m^{-3}). Therefore, SCOPE generally underestimates soil evaporation when soil moisture is higher than 0.25 and overestimates soil evaporation when it is lower than 0.25. Due to the lack of measurement of soil surface moisture in this study, we use the average soil moisture at root zone simulated by SCOPE_STEMMUS as the input data for SCOPE_SM to calculate soil surface resistance and soil evaporation. Although STEMUS can capture variation of soil evaporation reasonably well, it has higher *RMSE* value than SCOPE_STEMMUS. This is probably attributed to the comprehensive consideration of radiation transfer in SCOPE, which is lacking in STEMMUS. Consequently, the simulation of soil net radiation of the coupled model was more accurate than STEMMUS alone. The *RMSE* value of SCOPE_STEMMUS was 0.60 mm day^{-1}, which was lower than those of other three models (i.e. 0.67, 0.65, and 0.64 mm day^{-1} respectively). For SCOPE_STEMMUS, the major differences between simulations and observations occurred in rainy days, which may be caused by errors of soil surface resistance estimation during these periods or the uncertainty of ET partitioning method.

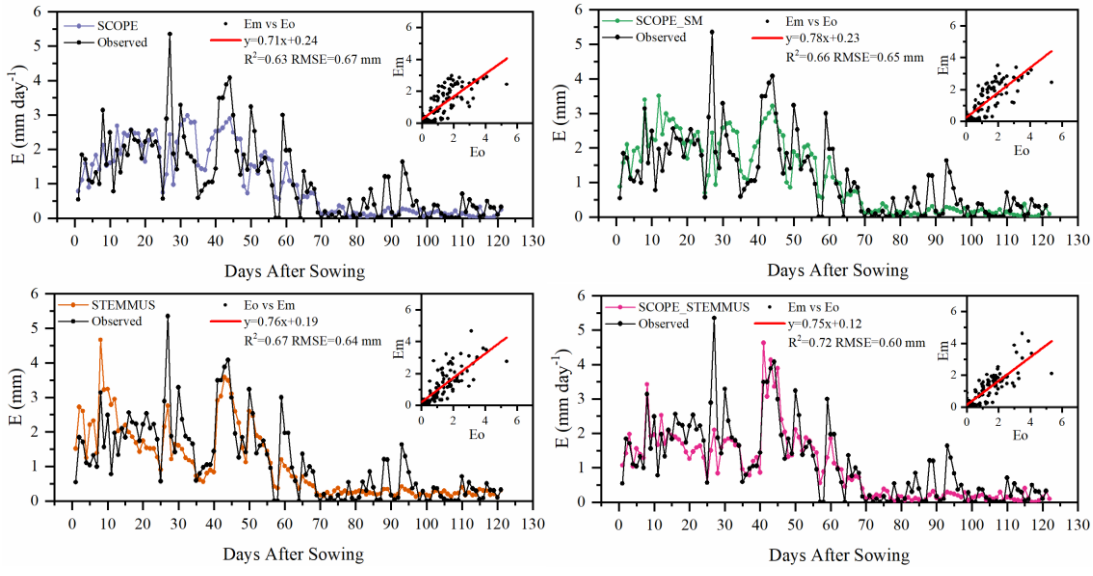

Figure 9 Comparison of observed and modeled daily soil evaporation (E) (Eo: observed E; Em: modeled E).

3.5. Daily NEE modeling

Simulated *NEE* by SCOPE, SCOPE_SM and SCOPE_STEMMUS and observed *NEE* were presented in Figure 10. As shown, similar to the simulation of transpiration, SCOPE cannot respond to water stress when simulating *NEE*. After introducing soil water stress factor in SCOPE_STEMMUS and SCOPE_SM, the simulations of *NEE* were improved in both models. The consistency between simulated and observed *NEE* at mid and late stages were higher than those at early and rapidly growth stages. The difference usually occurred when soil moisture increased. The reason is that the simulated *NEE*

https://doi.org/10.5194/gmd-2020-85
Preprint. Discussion started: 2 June 2020

Geoscientific Model Development Discussions

was calculated by *GPP* and *Re*, and *Re* was not only influenced by soil temperature, but also by soil moisture. However, in this study, we only considered the effect of soil temperature on *Re*. Many studies evidenced that soil respiration increased with increasing soil moisture, especially when rain or irrigation occurred. Generally, in the summer, soil temperature decreases when raining or irrigating. However, the model only considers the effect of reduced soil temperature on *Re*, while ignores the positive effect of increasing soil moisture. As such, the simulated soil respiration would decrease with soil temperature dropped. For the late stage, as soil moisture was stable and maintained at a high level, the difference between simulated and observed soil respiration was relatively small. This can also demonstrate that the errors of *NEE* simulation were mainly caused by the effect of soil moisture on soil respiration.

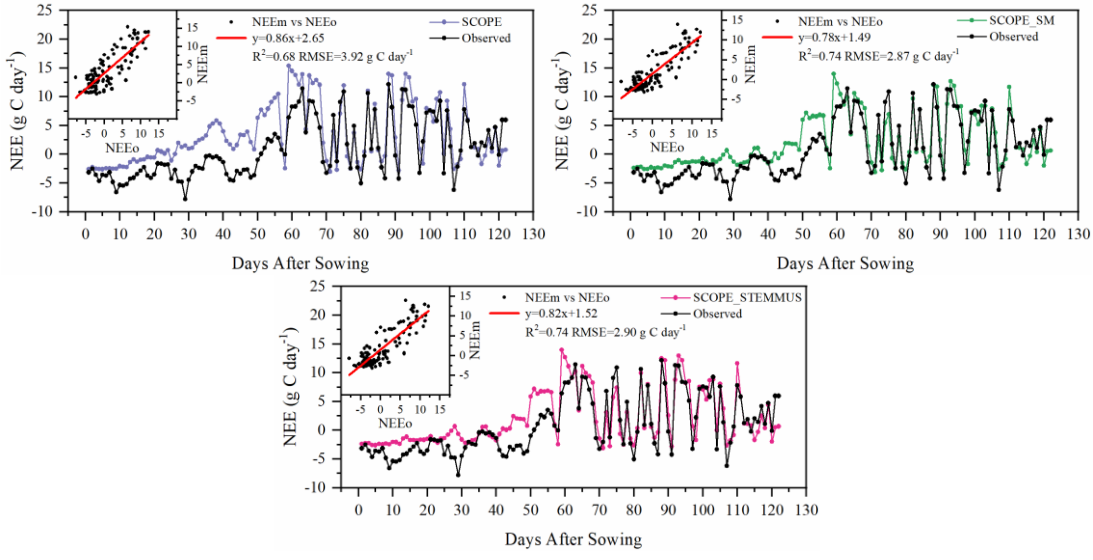

Figure 10 Comparison of observed and modeled daily net ecosystem exchange (NEE) (NEEo: observed NEE; NEEm: modeled NEE).

4. Discussion

4.1. Leaf water potential, water stress factor, and root length density

Leaf water potential was a parameter to reflect plant water status. The simulated half-hourly leaf water potential and water stress factor are presented in Figure 11. The leaf water potential was lower when vegetation suffering water stress compared to other periods. The reason is that soil water potential is low due to the low soil moisture and the leaves need to maintain an even lower water potential to suck water from the soil and transfer it to leaves. During mid and late stages, the leaf water potential was sensitive to transpiration demand due to the slowdown of root system growth. As the continuous measurements of the leaf water potential is not available, we compared the simulated leaf water potential to the measurements reported in other literatures.

https://doi.org/10.5194/gmd-2020-85
Preprint. Discussion started: 2 June 2020

Geoscientific Model Development Discussions

Many studies have measured midday leaf water potential or dawn leaf water potential. Fan et al. (2015) reported that the leaf water potential of well-watered maize was maintained high between -73 to -88 m and leaf water potential would decrease when soil water content was lower than 80% of field capacity. Martineau et al. (2017) reported the midday leaf water potential of well-watered maize was around -82 m and the midday leaf water potential decreased to -130 m when the maize was suffering water stress. Moreover, O'Toole and Cruz (1980) studied the response of leaf water potential to water stress in rice and concluded that the leaf water potential of rice can be lower than -80 to -120 m when the vegetation is under water stress and the leaves start curling, which was similar to the simulated leaf water potential of maize in this study. Aston and Lawlor (1979) revealed the relationship between transpiration, root water uptake and leaf water potential of maize. These field studies found that leaf water potential is often very low and it reaches valley values at midday. Elfving (1972) developed a water flux model, which was based on SPAC system and evaluated with the orange tree. In his study, the valley value of leaf water potential under non-limiting environmental conditions was about -120 m, which was slightly lower than the simulation in this study.

In this study, the calculation of water stress factor considered the effect of soil moisture and root distribution. The severe water stress was from DAS 30 to DAS 40, and the coupled model performed very well in this period. As the feedback, water stress can also influence root water uptake and root growth, and then influence soil moisture and root dynamic in the next time step. It indicates that the water stress equation used in this study can characterize the reduction of V_{cmax} reasonably well.

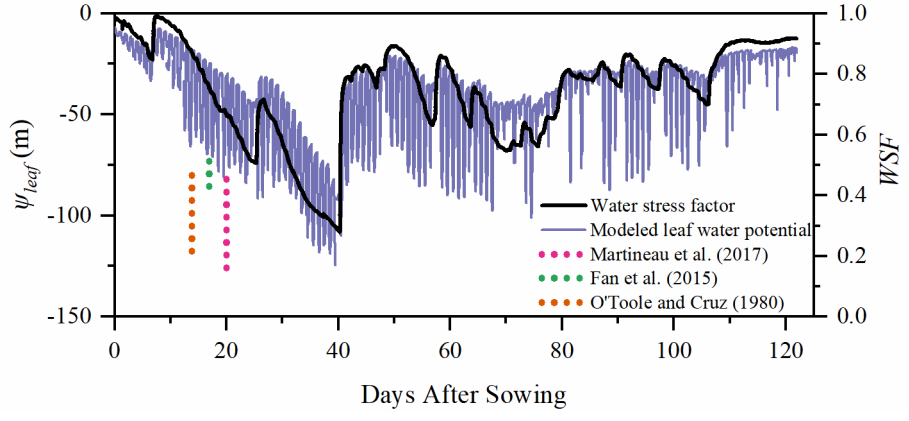

Figure 11 Simulation of ψ_{leaf} (leaf water potential, m) and *WSF* (water stress factor). (The dashed lines represent the range of midday leaf water potential reported in other sites.)

Root length density is another vital parameter in root water uptake calculation. As shown in Figure 12, the root length density was high from 10 to 20 cm depth and gradually decrease from 20 cm to 121 cm. Many previous studies have revealed that root length density was influenced by soil moisture, bulk density, tillage, and soil mineral nitrogen (Amato and Ritchie, 2002; Chassot et al., 2001; Schroder et al., 1996). In this study, as we assumed the soil was homogenous, SCOPE_STEMMUS considered the effect of soil moisture but neglected the effect of bulk density and soil mineral nitrogen.

https://doi.org/10.5194/gmd-2020-85
Preprint. Discussion started: 2 June 2020

Amato and Ritchie (2002) also found a similar result as this study about the root length density in a maize field. Peng et al. (2012) studied temporal and spatial dynamics in root length density of field-grown maize and found 80% root length density distributed at 0-30 cm depth with peak values from 0.86 to 1.00 cm cm^{-3}. Ning et al. (2015) also reported a similar observation of root length density. Chassot et al. (2001) and Qin et al. (2006) reported that root length density can reach 7 cm cm^{-3} at Swiss midlands. Aina and Fapohunda (1986) also found that root length density can reach 2.5 cm cm^{-3} if the maize was well-watered. In Stuttgart, Germany, Wiesler and Horst (1994) observed the root growth and nitrate utilization of maize under field condition. The observed root length density was 2.45-2.80 cm cm^{-3} at 0-30 cm depth which was much higher than in other studies, and decreased to 0.01 cm cm^{-3} at 120-150 cm depth, which was consistent with the observation of Oikeh et al. (1999) at Samaru, Nigeria. Zhuang et al. (2001b) proposed a scaling model to estimate the distribution of root length density of field grown maize. In their study, measured root length density in Tokyo, Japan decreased from 0.4-0.95 cm cm^{-3} at top soil layer to about 0.1 cm cm^{-3} at the bottom layer. Zhuang et al. (2001a) observed that the root length density of maize was mainly distributed at 0-60 cm depth and the maximum values were about 0.9 cm cm^{-3}. These studies indicate that the root length density values were quite variable when it was observed at different sites, nevertheless the simulated root length density was in order of magnitude similar to the observations in previous studies.

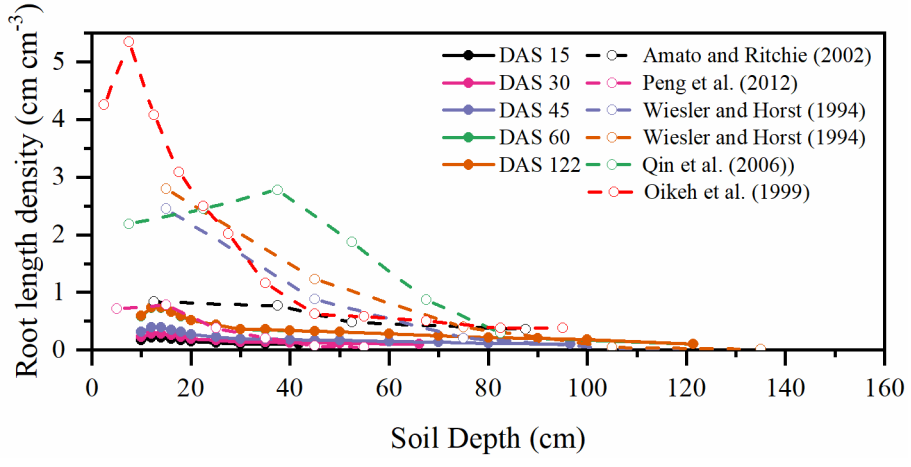

Figure 12 Simulation of root length density (m m^{-3}). (The dashed lines represent the measured root length density reported in other sites.)

5. Conclusions

A fundamental understanding of coupled energy, water and carbon flux is vital for obtaining the information of ecohydrological processes and functioning under climate change. The coupled model, SCOPE_STEMMUS, integrating radiative transfer, photochemistry, energy balance, root system dynamic, and soil moisture and soil temperature dynamic, has been proven to be a practical model to simulate detailed land surface processes such as evapotranspiration and NEE. In

https://doi.org/10.5194/gmd-2020-85
Preprint. Discussion started: 2 June 2020


Geoscientific Model Development Discussions

the coupled model, STEMMUS could provide root zone moisture profile to SCOPE, which was used to calculate water stress factor. On the other hand, SCOPE can provide soil surface temperature to STEMMUS, which was used subsequently as the top boundary condition. The performance of the coupled SCOPE_STEMMUS model in ET partitioning was improved due to the comprehensive radiative transfer scheme in SCOPE. The coupled model has been successfully applied in a maize field.

Through the inter-comparison of SCOPE, SCOPE_SM, STEMMUS, and SCOPE_STEMMUS, we concluded that the coupled STEMMUS_SCOPE can be used to investigate vegetation states under water stress conditions, and to simultaneously understand the dynamics of soil heat and mass transfer, as well as the root growth. However, there are some needs for further studies to enhance the capacity of STEMMUS_SCOPE in understanding ecosystem functioning. Frist of all, the estimation of soil boundary condition especially during the irrigation period, which has significant influence on the simulation of soil temperature, needs further improvement. Second, the soil respiration model used in SCOPE, which neglected currently the effect of soil moisture, should be upgraded in the coupled model. Nevertheless, the SCOPE_STEMMUS may be used as an observation operator to assimilate remote sensing data such as solar-induced chlorophyll fluorescence, to improve the estimation of water and carbon fluxes. SCOPE_STEMMUS could also be used to investigate regional or global land surface processes, especially in arid and semi-arid regions, due to its sensitivity to water stress conditions.

Code and data availability. The development and validation of SCOPE_STEMMUS in this paper were conducted in MATLAB R2016a. The exact version of the model used to produce the results used in this paper is archived on Zenodo (Wang et al., 2020). The original source of the SCOPE model and STEMMUS model was obtained from Van der Tol et al. (2009) and Zeng et al. (2011a, b), respectively. The tower-based eddy-covariance measurements used for model validation were obtained from the authors in Yangling, China (Wang et al., 2019).

Author contributions. YW, YZ, LY, PY, CV, ZS and HC designed the study, Developed the code, conducted the analysis, and wrote the manuscript with YW and HC collected and shared their eddy-covariance measurements for the purpose of model validation. All authors gave comments and contributed to the final version of the manuscript.

Competing interests. The authors declare that they have no conflict of interest.

Acknowledgments. This work was supported by the National Natural Science Foundation of China (51879223 and 41971033), the National Key Research and Development Program of China (2016YFC0400201), the Fundamental Research Funds for the Central Universities, CHD (300102298307), and China Scholarship Council.

https://doi.org/10.5194/gmd-2020-85
Preprint. Discussion started: 2 June 2020

Geoscientific Model Development Discussions

Appendix A

A.1. Water Stress Factor in SCOPE

The C4 Photosynthesis is calculated in the SCOPE model as the minimum of three processes (Farquhar et al., 1980); (1) carboxylation rate limited by Ribulose biphosphate-carboxylase-oxygenase activity (known as Rubisco (enzyme)-limited, V_c, described in Eq. (A1); (2) carboxylation rate limited by Ribulose 1–5 bisphosphate regeneration rate (known as RuBP (electron transport/light)-limited), V_e, described in Eq. (A2); (3) At low CO_2 concentrations, carboxylation rate limited by intercellular CO_2 partial pressure (p_i), V_s, described in Eq. (A3).

$$V_c = V_{cmax} * WSF \tag{A1}$$

$$V_e = \frac{J}{6}\frac{-b\pm\sqrt{b^2-4ac}}{2a} \tag{A2}$$

$$V_s = p_i(k_p - \frac{L}{p_i})/P \tag{A3}$$

$$A_n = min(V_c, V_e, V_s) \tag{A4}$$

$$C_i = C_a(1 - \frac{1}{mRH}) \tag{A5}$$

where V_{cmax} is the maximum carboxylation rate (μmol m^{-2} s^{-1}), p_i is the intercellular CO_2 partial pressure (Pa), k_p is a pseudo-first-order rate constant for PEP carboxylase with respect to C_i, P is the atmospheric pressure; A_n is the net photosynthesis (μmol m^{-2} s^{-1}); *WSF* is the total water stress factor, J is the electron transport rate (μmol m^{-2} s^{-1}), C_i is the intercellular CO_2 concentration (μmol m^{-3}) and C_a is CO_2 concentration in the boundary layer (μmol m^{-3}), m is Ball-Berry parameter and RH is relative humidity at the leaf surface (%).

In the study of Bayat et al. (2019), water stress factor was calculated based on the root zone soil moisture content neglecting the distribution of root length. In this study, water stress factor considered both root length distribution and water content in root zone. We use a sigmoid formulation rather than the piecewise function by Bayat et al. (2019). The calculations are as follows:

$$WSF = \sum_{i=1}^{n} RF(i) * WSF\ (i) \tag{A6}$$

$$WSF(i) = \frac{1}{1+e^{-100*\theta_{sat}\left(SM(i)-\frac{\theta_f+\theta_r}{2}\right)}} \tag{A7}$$

θ_r is the soil water content at wilting point; θ_f is the soil water content at field capacity; θ_{sat} is the saturated soil water content; *WSF(i)* is the water stress factor at each soil layer; *RF(i)* is the ratio of *root length* in soil layer *i* and its calculation can be found in the appendix A.4; *SM(i)* is the soil moisture at each soil layer.

https://doi.org/10.5194/gmd-2020-85
Preprint. Discussion started: 2 June 2020


Geoscientific Model Development Discussions

A.2. Governing Equations in STEMMUS

A.2.1 Soil water conservation equation

$$\frac{\partial}{\partial t}(\rho_L\theta_L+\rho_V\theta_V)=-\frac{\partial}{\partial z}(q_{Lh}+q_{LT}+q_{La}+q_{Vh}+q_{VT}+q_{Va})-S=\rho_L\frac{\partial}{\partial z}\left[K\left(\frac{\partial h}{\partial z}+1\right)+D_{TD}\frac{\partial T_s}{\partial z}+\frac{K}{\gamma_w}\frac{\partial P_g}{\partial z}\right]+$$
$$\frac{\partial}{\partial z}\left[D_{Vh}\frac{\partial h}{\partial z}+D_{VT}\frac{\partial T_s}{\partial z}+D_{Va}\frac{\partial P_g}{\partial z}\right]-S \quad \text{(A8)}$$

where ρ_L, ρ_V (kg m^{-3}) are the density of liquid water, water vapor, respectively; q_L , q_V (m^3 m^{-3}) are the volumetric water content (liquid and water vapor, respectively); z (m) is the vertical space coordinate (positive upwards); S (cm s^{-1}) is the sink term for the root water extraction. K (m s^{-1}) is hydraulic conductivity; h (cm) is the pressure head; T_s (°C) is the soil temperature; and P_g (Pa) is the mixed pore-air pressure. γ_w (kg m^{-2} s^{-2}) is the specific weight of water. D_{TD} (kg m^{-1} s^{-1} °C^{-1}) is the transport coefficient for adsorbed liquid flow due to temperature gradient; D_{Vh} (kg m^{-2} s^{-1}) is the isothermal vapor conductivity; and D_{VT} (kg m^{-1} s^{-1} °C^{-1}) is the thermal vapor diffusion coefficient. D_{Va} is the advective vapor transfer coefficient (Zeng et al. 2011a,b). q_{Lh}, q_{LT}, and q_{La}(kg m^{-2} s^{-1}) are the liquid water fluxes driven by the gradient of matric potential, temperature, and air pressure, respectively. q_{Vh}, q_{VT}, and q_{Va} (kg m^{-2} s^{-1}) are the water vapor fluxes driven by the gradient of matric potential, temperature, and air pressure, respectively.

A.2.2 Dry air conservation equation

$$\frac{\partial}{\partial t}[\varepsilon\rho_{da}(S_a+H_cS_L)]=\frac{\partial}{\partial z}\left[D_e\frac{\partial\rho_{da}}{\partial z}+\rho_{da}\frac{S_aK_g}{\mu_a}\frac{\partial P_g}{\partial z}-H_c\rho_{da}\frac{q_L}{\rho_L}+\left(\theta_aD_{Vg}\right)\frac{\partial\rho_{da}}{\partial z}\right] \quad \text{(A9)}$$

where ε is the porosity; ρ_{da} (kg m^{-3}) is the density of dry air; S_a (=1-S_L) is the degree of air saturation in the soil; S_L (=θ_L/ε) is the degree of saturation in the soil; H_c is Henry's constant; D_e (m^2 s^{-1}) is the molecular diffusivity of water vapor in soil; K_g (m^2) is the intrinsic air permeability; m_a (kg m^{-2} s^{-1}) is the air viscosity; q_L (kg m^{-2} s^{-1}) is the liquid water flux; θ_a (=θ_V) is the volumetric fraction of dry air in the soil; and D_{Vg} (m^2 s^{-1}) is the gas phase longitudinal dispersion coefficient (Zeng et al., 2011a,b).

A.2.3 Energy balance equation

$$\frac{\partial}{\partial t}[(\rho_s\theta_sC_s+\rho_L\theta_LC_L+\rho_V\theta_VC_V+\rho_{da}\theta_aC_a)(T_s-T_r)+\rho_V\theta_VL_0]-\rho_LW\frac{\partial\theta_L}{\partial t}=\frac{\partial}{\partial z}\left(\lambda_{eff}\frac{\partial T}{\partial z}\right)-\frac{\partial}{\partial z}[q_LC_L(T_s-T_r)+$$
$$q_V(L_0+C_V(T_s-T_r))+q_aC_a(T_s-T_r)]-C_LS(T_s-T_r) \quad \text{(A10)}$$

where C_s, C_L, C_V, C_a (J kg^{-1} °C^{-1}) are the specific heat capacities of solids, liquid, water vapor, and dry air, respectively; ρ_s(kg m^{-3}), ρ_L (kg m^{-3}), ρ_V (kg m^{-3}), and ρ_{da} (kg m^{-3}) are the density of solids, liquid water, water vapor, and dry air, respectively; θ_s is the volumetric fraction of solids in the soil; θ_L, θ_V, and θ_a are the volumetric fraction of liquid water, water vapor, and dry air, respectively; T_r (°C) is the reference temperature; L_0 (J kg^{-1}) is the latent heat of vaporization of

https://doi.org/10.5194/gmd-2020-85
Preprint. Discussion started: 2 June 2020


Geoscientific Model Development Discussions

water at temperature T_r; W (J kg^{-1}) is the differential heat of wetting (the amount of heat released when a small amount of free water is added to the soil matrix); and λ_{eff} (W m^{-1} °C^{-1}) is the effective thermal conductivity of the soil; q_L, q_V, and q_a (kg m^{-2} s^{-1}) are the liquid, vapor water and dry air flux.

A.3. Dynamic Root Growth Modelling

A.3.1. Root front growth

The depth of the root front is firstly initialized either with the sowing depth for sown crops or with an initial value for transplanted crops or perennial crops. The root front growth stops when it reached certain depth of soil or a physical/chemical obstacle preventing root growth, but also stops when the phenological stopping stage has been reached.

$$\Delta Z = \begin{cases} 0 & T_{air} < T_{min} \\ (T_{air} - T_{min}) * RGR & T_{min} < T_{air} < T_{max} \\ (T_{max} - T_{min}) * RGR & T_{max} < T_{air} \end{cases} \quad \text{(A11)}$$

$$D_Z(t) = D_Z(t-1) + \Delta Z \quad \text{(A12)}$$

where ΔZ is root front growth at t-th time step; D_Z (cm) is root zone depth; T_{air} (^{0}C) is air temperature; T_{min} (^{0}C) is the minimum temperature of root growth; T_{max} (^{0}C) is the maximum temperature of root growth; RGR (cm ^{0}C^{-1} day^{-1}) is the root growth rate of root front.

A.3.2. Root length growth

In this study, the root distribution in the root zone was realized via simulating the root length growth in each soil layer.

$$\Delta Rl\_tot = \frac{A_n * fr_{root}}{R_C * R_D * \pi * r_{root}^2} \quad \text{(A13)}$$

fr_{root} is the allocation fraction of net assimilation to root, and fr_{root} is assumed as a function of leaf area index (LAI) and root zone water content. A_n is the net assimilation rate (μmol m^{-2} s^{-1}). R_C is ratio of carbon to dry organic matter in root, R_D is root length density (m), and r_{root} is radius of the root (0.15*10^{-3} m), and ΔRl_tot (m m^{-3}) is total root length growth.

The limiting factors for allocation are preliminarily computed and they account for root zone soil moisture availability A_W, and light availability A_L.

$$A_W = max[0.1, \quad min(1, \quad WSF)] \quad \text{(A14)}$$

where WSF is the averaged soil moisture stress factor in the root zone.

$$A_L = max[0.1, \quad e^{-K_e\, LAI}] \quad \text{(A15)}$$

where $K_e = 0.15$ is a constant light extinction coefficient.

https://doi.org/10.5194/gmd-2020-85
Preprint. Discussion started: 2 June 2020


Geoscientific Model Development Discussions

$$fr_{root} = max\left[r_{min},\quad r_0 \frac{3A_L}{A_L+2A_W}\right] \tag{A16}$$

where $r_{min}(= 0.15)$ is the minimum allocation coefficient to fine roots, and r_0 is a coefficient that indicates the theoretically unstressed allocation to fine roots.

$$\Delta Rl(i) = \Delta Rl\_tot * RF(i) \tag{A17}$$

where $RF(i)$ is the allocation fraction of root growth length in layer i, $\Delta Rl(i)$ is the root growth length in layer i.

$$Rl_i^t = Rl_i^{t-1} + \Delta Rl(i) \tag{A18}$$

where Rl_i^t and Rl_i^{t-1} is the root length of layer i at time step t and time step t-1.

$$RF(i) = \frac{Rl(i)}{Rl_T} \tag{A19}$$

where Rl_T is the total root length in root zone, $Rl(i)$ is the root length in soil layer i.

A.4. Root water uptake

The equation to calculate root water uptake and transpiration was as follows:

$$\sum_{i=1}^{n} \frac{\psi_{s,i}-\psi_l}{r_{s,i}+r_{r,i}+r_{x,i}} = \frac{0.622}{P}\frac{\rho_{da}}{\rho_V}\left(\frac{e_l-e_a}{r_c+r_a}\right) = T \tag{A20}$$

where $\psi_{s,i}$ is soil water potential of layer i (m), ψ_l is leaf water potential (m), $r_{s,i}$ is the soil hydraulic resistance (s m^{-1}), $r_{r,i}$ is the root resistance to water flow radially across the roots (s m^{-1}), and $r_{x,i}$ is the plant axial resistance to flow from the soil to the leaves (s m^{-1}). e_l and e_a are vapor pressure of leaf and the atmosphere (hPa), respectively, and r_a and r_c are aerodynamic resistance and canopy resistance (s m^{-1}), respectively. ρ_{da} is the density of dry air (kg m^{-3}). ρ_V is the density of water vapor. P is the atmospheric pressure (Pa). 0.622 is the ratio of the molar mass of water to air.

$\psi_{s,i}$ is described as a function of soil moisture by Van Genuchten (1980), and the relevant parameters were shown in Table B.1.

The r_s is calculated by Reid and Huck (1990) as:

$$r_s = \frac{1}{B \cdot K \cdot R_D \cdot \Delta d} \tag{A21}$$

where B is the root length activity factor, K is hydraulic conductivity of soil (m s^{-1}), R_D is root length density (m m^{-3}), and Δd is the thickness of the soil layer (m). B is calculated as:

https://doi.org/10.5194/gmd-2020-85
Preprint. Discussion started: 2 June 2020


Geoscientific Model Development Discussions

$$B = \frac{2\pi}{ln[(\pi R_D)^{-1/2}/r_{root}]} \quad \text{(A22)}$$

where r_{root} is root radius (m).

The r_r is estimated as (Reid and Huck, 1990):

$$r_r = \frac{P_r(\theta_{sat}/\theta)}{L_v \Delta d} \quad \text{(A23)}$$

where P_r is root radial resistivity (s m^{-1}).

The xylem resistance r_x is estimated by Klepper et al. (1983):

$$r_x = \frac{P_a Z_{mid}}{0.5 f L_v} \quad \text{(A24)}$$

where P_a is root axial resistivity (s m^{-3}), Z_{mid} is the depth of the midpoint of soil layer, and f is a fraction defined for a specific depth as the number of roots which connect directly to the stem base to total roots crossing a horizontal plane at that depth. We can consider it equal to 0.22 based on Klepper et al. (1983).

The updated root water uptake term is:

$$S_i = \frac{\psi_{s,i} - \psi_l}{r_{s,i} + r_{r,i} + r_{x,i}} \quad \text{(A25)}$$

Different from other studies which need to calculate the compensotary water uptake and hydraulic redistribution after calculating the standard water uptake of each soil layer, the sink term in this study is calculated by a physically-based model which contain the effect of root resistance and soil hydraulic resistance rather than only considering the root fraction, so the compensary uptake and hydraulic redistribution have been considered when calcualting the sink term.

https://doi.org/10.5194/gmd-2020-85
Preprint. Discussion started: 2 June 2020


Geoscientific Model Development Discussions

Appendix B.

Table B.1 List of parameters and values used in this study (All the parameters were classified as Air, Canopy, Root and Soil).

Symbol	Description	Unit	Value
Aerodynamic			
aPAR	Absorbed photosynthetically active radiation	μmol m^{-2} s^{-1}	
e_a	Air vapor pressure	Pa	
e_l	Vapor pressure of leaf	hPa	
P	Air pressure	Pa	
q_a	Humidity above the canopy	kg m^{-3}	
q_l	Humidity in stomata	kg m^{-3}	
r_a	Aerodynamic resistance	s m^{-1}	
RH	Relative humidity	%	
R_{li}	Incoming longwave radiation	W m^{-2}	
R_{in}	Incoming shortwave radiation	W m^{-2}	
R_n	Net radiation	W m^{-2}	
T_{air}	Air temperature	^{0}C	
u	Wind speed	m s^{-1}	
VPD	Vapor pressure deficit	hPa	
Canopy			
A_n	Net assimilation rate	μmol m^{-2} s^{-1}	
C_a	CO_2 concentration in the boundary layer	μmol m^{-3}	
C_{ab}	Leaf chlorophyll content	μg cm^{-2}	80
C_{ca}	Leaf Carotenoid content	μg cm^{-2}	20
C_w	Leaf water content	g cm^{-2}	0.009
C_{dm}	Leaf dry matter content	g cm^{-2}	0.012
C_s	Senescent material content		0
DAS	Days after sowing	d	
ET	Evapotranspiration	mm day^{-1}	
GPP	Gross primary production	g C m^{-2} day^{-1}	
h_c	Canopy height	m	[0-1.95]
H	Sensible heat flux	W m^{-2}	
J	Electron transport rate	μmol m^{-2} s^{-1}	150

https://doi.org/10.5194/gmd-2020-85
Preprint. Discussion started: 2 June 2020


Geoscientific Model Development Discussions

K_e	Light extinction coefficient		0.15
k_p	A pseudo-first-order rate constant for PEP carboxylase		
LAI	Leaf area index	$m^2\ m^{-2}$	[0-4.39]
LIDF	Leaf inclination distribution function		[-1, 0]
LE	Latent heat flux	$W\ m^{-2}$	
LE_c	Latent heat flux of canopy	$W\ m^{-2}$	
m	Ball-Berry stomatal conductance parameter		4
NEE	Net ecosystem exchange	$g\ C\ m^{-2}\ day^{-1}$	
p_i	Intercellular CO_2 partial pressure	Pa	
r_c	Canopy resistance	$s\ m^{-1}$	
Re	Ecosystem respiration	$g\ C\ m^{-2}\ day^{-1}$	
T	Transpiration	$mm\ day^{-1}$	
T_c	Vegetation temperature	^0C	
T_{ch}	Leaf temperature (shaded leaves)	^0C	
T_{cu}	Leaf temperature (sunlit leaves)	^0C	
$uWUE_p$	Potential water use efficiency	$g\ C\ hPa^{0.5}/kg\ H_2O$	
uWUE	Water use efficiency	$g\ C\ hPa^{0.5}/kg\ H_2O$	
V_{cmax}	Maximum carboxylation rate	$\mu mol\ m^{-2}\ s^{-1}$	50
ψ_l	Leaf water potential	m	
Root			
A_W	Root zone soil moisture availability		
A_L	Light availability		
B	Root length activity factor		
D_Z	Root zone depth	cm	
f	A fraction defined for a specific depth as the number of roots which connect directly to the stem base to total roots crossing a horizontal plane at that depth		0.22
fr_{root}	Allocation fraction of net assimilation to root		
P_a	Root axial resistivity	$s\ m^{-3}$	$1*10^{10}$
P_r	Root radial resistivity	$s\ m^{-1}$	$0.65*10^{12}$
RF(i)	The allocation fraction of root growth length in layer *i*		
Rl_T	Total root length in root zone	m	
Rl_i^t	Root length of layer *i* at time step *t*	m	

https://doi.org/10.5194/gmd-2020-85
Preprint. Discussion started: 2 June 2020


Geoscientific Model Development Discussions

Rl_i^{t-1}	Root length of layer *i* at time step *t-1*	m	
Rl(i)	Root length in soil layer *i*	m	
RGR	Root growth rate of front	cm ^{0}C day^{-1}	0.002
R_D	Root length density	m m^{-3}	
r_{min}	The minimum allocation coefficient to fine roots		0.15
r_0	Coefficient of theoretically unstressed allocation to fine roots		0.3
r_{root}	Radius of the root	m	0.15*10^{-3}
$r_{x,i}$	Plant axial resistance to flow from the soil to the leaves	s	
$r_{r,i}$	Resistance to water flow radially across the roots	s	
$r_{s,i}$	Soil hydraulic resistance	s	
R_C	Ratio of carbon to dry organic matter in root	kg kg^{-1}	0.488
RWU	Root water uptake	m s^{-1}	
RF(i)	The ratio of root length in soil layer *i*		
T_{min}	Minimum temperature of root growth	^{0}C	10
T_{max}	Maximum temperature of root growth	^{0}C	40
$\triangle Z$	Root front growth at *t*-th step	cm	
$\triangle Rl\_tot$	Total root length growth	m	
$\triangle Rl(i)$	The root growth length in layer *i*	m	
Soil			
C_s	Specific heat capacities of solids	J kg^{-1} °C^{-1}	
C_L	Specific heat capacities of liquid	J kg^{-1} °C^{-1}	4.186*10^3
C_V	Specific heat capacities of water vapor	J kg^{-1} °C^{-1}	1.870*10^3
C_a	Specific heat capacities of dry air	J kg^{-1} °C^{-1}	1.255*10^{-3}
D_{TD}	Transport coefficient for absorbed liquid flow due to temperature gradient	kg m^{-1} s^{-1} °C^{-1}	
D_{Vh}	Isothermal vapor conductivity	kg m^{-2} s^{-1}	
D_{VT}	Thermal vapor diffusion coefficient	kg m^{-1} s^{-1} °C^{-1}	
D_{Va}	Advective vapor transfer coefficient	kg m^{-2} s^{-1}	
D_{Vg}	Gas phase longitudinal dispersion coefficient	m^2 s^{-1}	
D_e	Molecular diffusivity of water vapor in soil	m^2 s^{-1}	
E	Soil evaporation	mm	

https://doi.org/10.5194/gmd-2020-85
Preprint. Discussion started: 2 June 2020

Geoscientific Model Development Discussions

G	Soil heat flux	W m^{-2}	
h	Soil matric potential	cm	
H_c	Henry's constant		0.02
K	Hydraulic conductivity	m s^{-1}	
K_g	Intrinsic air permeability	m^2	
K_s	Saturation hydraulic conductivity	cm day^{-1}	18
LE_s	Latent heat flux of soil	W m^{-2}	
L_0	Latent heat of vaporization of water temperature T_r	J kg^{-1}	2497909
m_a	Air viscosity	kg m^{-1} s^{-1}	$1.846*10^{-5}$
n	Soil-dependent parameter		1.41
P_g	Mixed pore-air pressure	Pa	
q_L	Liquid water flux	kg m^2 s^{-1}	
q_{Lh}	Liquid water flux driven by the gradient of matric potential	kg m^2 s^{-1}	
q_{LT}	Liquid water flux driven by the gradient of temperature	kg m^2 s^{-1}	
q_{La}	Liquid water flux driven by the gradient of air pressure	kg m^2 s^{-1}	
q_V	Water vapor flux	kg m^2 s^{-1}	
q_{Vh}	Water vapor flux driven by the gradient of matric potential	kg m^2 s^{-1}	
q_{VT}	Water vapor flux driven by the gradient of temperature	kg m^2 s^{-1}	
q_{Va}	Water vapor flux driven by the gradient of air pressure	kg m^2 s^{-1}	
q_a	Dry air flux	kg m^2 s^{-1}	
S	Sink term for the root water extraction	cm s^{-1}	
S_a	Degree of air saturation in the soil		
S_L	Degree of saturation in the soil		
$SM(i)$	The soil moisture at a specific soil layer	m^3 m^{-3}	
T_s	Soil temperature	^{0}C	
T_{s0}	Soil surface temperature	^{0}C	
T_r	Reference temperature	°C	20
W	Differential heat of wetting	J kg^{-1}	$1.001*10^3$
WSF	Total water stress factor		
$WSF(i)$	Water stress factor at a specific soil layer		
Z_{mid}	The depth of the midpoint of soil layer	m	
$\triangle d$	Thickness of the soil layer	m	
α	Soil-dependent parameter	m^{-1}	0.45

https://doi.org/10.5194/gmd-2020-85
Preprint. Discussion started: 2 June 2020


Geoscientific Model Development Discussions
Open Access
EGU

θ_{sat}	Saturated water content	$m^3\ m^{-3}$	0.42
θ_f	Field capacity	$m^3\ m^{-3}$	0.272
θ_r	Residual water content	$m^3\ m^{-3}$	0.0875
θ	Volumetric soil water content	$m^3\ m^{-3}$	
θ_L	Volumetric moisture content	$m^3\ m^{-3}$	
θ_V	Volumetric vapor content	$m^3\ m^{-3}$	
θ_s	Volumetric fraction of solids in the soil	$m^3\ m^{-3}$	
θ_a	Volumetric fraction of dry air in the soil	$m^3\ m^{-3}$	
$\psi_{s,i}$	Soil water potential of layer *i*	m	
ψ_{soil}	Soil water potential	m	
λ_{eff}	Effective thermal conductivity of the soil	$W\ m^{-1}\ °C^{-1}$	
γ_w	Specific weight of water	$kg\ m^{-2}\ s^{-2}$	
ρ_{da}	Density of dry air	$kg\ m^{-3}$	
ρ_V	Density of vapor	$kg\ m^{-3}$	
ρ_L	Density of liquid water	$kg\ m^{-3}$	1
ρ_s	Density of solids	$kg\ m^{-3}$	
ε	Soil porosity	$m^3\ m^{-3}$	0.50

https://doi.org/10.5194/gmd-2020-85
Preprint. Discussion started: 2 June 2020


Geoscientific Model Development Discussions

References

Aina, P. and Fapohunda, H.: Root distribution and water uptake patterns of maize cultivars field-grown under differential irrigation, Plant Soil, 94, 257-265, https://doi.org/10.1007/bf02374349, 1986.

Amato, M. and Ritchie, J.T.: Spatial distribution of roots and water uptake of maize (Zea mays L.) as affected by soil structure, Crop Sci., 42, 773-780, https://doi.org/10.2135/cropsci2002.7730, 2002.

Amenu, G. and Kumar, P.: A model for hydraulic redistribution incorporating coupled soil-root moisture transport, Hydrol. Earth Syst. Sci., 4, 3719-3769, https://doi.org/10.5194/hessd-4-3719-2007, 2007.

Aston, M. and Lawlor, D.W.: The relationship between transpiration, root water uptake, and leaf water potential, J. Exp. Bot., 30, 169-181, https://doi.org/10.1093/jxb/30.1.169, 1979.

Bayat, B., Van der Tol, C., and Verhoef, W.: Integrating satellite optical and thermal infrared observations for improving daily ecosystem functioning estimations during a drought episode, Remote Sens. Environ., 209, 375-394, https://doi.org/10.1016/j.rse.2018.02.027, 2018.

Bayat, B., Van der Tol, C., Yang, P., and Verhoef, W.: Extending the SCOPE model to combine optical reflectance and soil moisture observations for remote sensing of ecosystem functioning under water stress conditions, Remote Sens. Environ., 221, 286-301, https://doi.org/10.1016/j.rse.2018.11.021, 2019.

Beaudoin, N., Mary, B., Launay, M., and Brisson, N.: Conceptual basis, formalisations and parameterization of the STICS crop model, Quae, 2009.

Bingham, I.J. and Wu, L.: Simulation of wheat growth using the 3D root architecture model SPACSYS: validation and sensitivity analysis, Eur. J. Agron., 34, 181-189, https://doi.org/10.1016/j.eja.2011.01.003, 2011.

Caldwell, M.M., Dawson, T.E., and Richards, J.H.: Hydraulic lift: consequences of water efflux from the roots of plants, Oecologia, 113, 151-161, https://doi.org/10.1007/s004420050363, 1998.

Camargo, G. and Kemanian, A.: Six crop models differ in their simulation of water uptake, Agric. For. Meteorol., 220, 116-129, https://doi.org/10.1016/j.agrformet.2016.01.013, 2016.

Chassot, A., Stamp, P., and Richner, W.: Root distribution and morphology of maize seedlings as affected by tillage and fertilizer placement, Plant Soil, 231, 123-135, https://doi.org/10.1023/A:1010335229111, 2001.

Couvreur, V., Vanderborght, J., and Javaux, M.: A simple three-dimensional macroscopic root water uptake model based on the hydraulic architecture approach, Hydrol. Earth Syst. Sci., 16, 2957-2971, https://doi.org/10.5194/hess-16-2957-2012, 2012.

Deng, Z., H. Guan, J. Hutson, M. A. Forster, Y. Wang, and C. T. Simmons.: A vegetation focused soil-plant-atmospheric continuum model to study hydrodynamic soil-plant water relations, Water Resour. Res., 53, 4965– 4983, doi:10.1002/2017WR020467, 2017.

Elfving, D. C., KAUFMANN, M. R., and HALL, A. E.: Interpreting leaf water potential measurements with a model of the soil-plant-atmosphere continuum, Physiol. Plant., 27(2), 161-168, https://doi.org/10.1111/j.1399-3054.1972.tb03594.x, 1972.

Espeleta, J., West, J., and Donovan, L.: Species-specific patterns of hydraulic lift in co-occurring adult trees and grasses in a sandhill community, Oecologia, 138, 341-349, https://doi.org/10.1007/s00442-004-1539-x, 2004.

Fan, X., Hu, H., Huang, G., Huang, F., Li, Y., and Palta, J.: Soil inoculation with Burkholderia sp. LD-11 has positive effect on water-use efficiency in inbred lines of maize, Plant and Soil 390, 337-349, https://doi.org/10.1007/s11104-015-2410-z, 2015.

Farquhar, G.D., von Caemmerer, S., and Berry, J.A.: A biochemical model of photosynthetic

CO_2 assimilation in leaves of C3 species, Planta, 149, 78–90, https://doi.org/10.1007/bf00386231, 1980.

Fu, C., Wang, G., Goulden, M.L., Scott, R.L., Bible, K., and G Cardon, Z.: Combined measurement and modeling of the hydrological impact of hydraulic redistribution using CLM4. 5 at eight AmeriFlux sites, Hydrol. Earth Syst. Sci., 20, https://doi.org/10.5194/hess-2016-24-rc1, 2016.

Guo, Y.: Simulation of water transport in the soil-plant-atmosphere system, https://doi.org/10.31274/rtd-180813-9473, 1992.

Jarvis, N.: Simple physics-based models of compensatory plant water uptake: Concepts and eco-hydrological consequences, Hydrol. Earth Syst. Sci., 15, 3431-3446, https://doi.org/10.5194/hess-15-3431-2011, 2011.

Jones, J.W., Hoogenboom, G., Porter, C.H., Boote, K.J., Batchelor, W.D., Hunt, L., Wilkens, P.W., Singh, U., Gijsman, A.J., and Ritchie, J.T.: The DSSAT cropping system model, Eur. J. Agron., 18, 235-265, https://doi.org/10.1016/s1161-0301(02)00107-7, 2003.

Keating, B.A., Carberry, P.S., Hammer, G.L., Probert, M.E., Robertson, M.J., Holzworth, D., Huth, N.I., Hargreaves, J.N., Meinke, H., and Hochman, Z.: An overview of APSIM, a model designed for farming systems simulation, Eur. J. Agron., 18, 267-288, https://doi.org/10.1016/s1161-0301(02)00108-9, 2003.

Klepper, B., Rickman, R.W., and Taylor, H.M.: Farm management and the function of field crop root systems, Agric. Water Manage., 7, 115–141, https://doi.org/10.1016/0378-3774(83)90078-1, 1983.

https://doi.org/10.5194/gmd-2020-85
Preprint. Discussion started: 2 June 2020


Geoscientific Model Development Discussions

Krinner, G., N. Viovy, N. de Noblet-Ducoudre, J. Ogee, J. Polcher, P. Friedlingstein, P. Ciais, S. Sitch, and I. C. Prentice.: A dynamic global vegetation model for studies of the coupled atmosphere-biosphere system, Glob. Biogeochem. Cycle, 19 (GB1015), doi:10.1029/2003GB002199, 2005.

Leitner, D., Klepsch, S., Bodner, G., and Schnepf, A.: A dynamic root system growth model based on L-Systems, Plant Soil, 332, 177-192, https://doi.org/10.1007/s11104-010-0284-7, 2010.

Li, L., Wang YP, Yu, Q., Pak, B., Eamus, D., and Yan, J.: Improving the responses of the australian community land surface model (cable) to seasonal drought, J. Geophys. Res.-Biogeosci., 117(G4), https://doi.org/10.1029/2012jg002038, 2012.

Martineau, E., Domec, J.-C., Bosc, A., Denoroy, P., Fandino, V.r.A., Lavres Jr, J., and Jordan-Meille, L.: The effects of potassium nutrition on water use in field-grown maize (Zea mays L.), Environ. Exp. Bot., 134, 62-71, https://doi.org/10.1016/j.envexpbot.2016.11.004, 2017.

Ning, P., Li, S., White, P.J., and Li, C.: Maize varieties released in different eras have similar root length density distributions in the soil, which are negatively correlated with local concentrations of soil mineral nitrogen, PLOS one, 10, e0121892, https://doi.org/10.1371/journal.pone.0121892, 2015.

O'Toole, J.C. and Cruz, R.T.: Response of leaf water potential, stomatal resistance, and leaf rolling to water stress, Plant Physiol., 65, 428-432, https://doi.org/10.1104/pp.65.3.428, 1980.

Oikeh, S., Kling, J., Horst, W., Chude, V., and Carsky, R.: Growth and distribution of maize roots under nitrogen fertilization in plinthite soil, Field Crop. Res., 62, 1-13, https://doi.org/10.1016/s0378-4290(98)00169-5, 1999.

Peng, Y., Yu, P., Zhang, Y., Sun, G., Ning, P., Li, X., and Li, C.: Temporal and spatial dynamics in root length density of field-grown maize and NPK in the soil profile, Field Crop. Res., 131, 9-16, https://doi.org/10.1016/j.fcr.2012.03.003, 2012.

Qin, R., Stamp, P., and Richner, W.: Impact of tillage on maize rooting in a Cambisol and Luvisol in Switzerland, Soil Tillage Res., 85, 50-61, https://doi.org/10.1016/j.still.2004.12.003, 2006.

Reichstein, M., Falge, E., Baldocchi, D., Papale, D., Aubinet, M., Berbigier, P., Bernhofer, C., Buchmann, N., Gilmanov, T., and Granier, A.: On the separation of net ecosystem exchange into assimilation and ecosystem respiration: review and improved algorithm, Glob. Change Biol., 11, 1424-1439, https://doi.org/10.1111/j.1365-2486.2005.001002.x, 2005.

Richards, J.H. and Caldwell, M.M.: Hydraulic lift: substantial nocturnal water transport between soil layers by Artemisia tridentata roots, Oecologia, 73, 486-489, https://doi.org/10.1007/bf00379405, 1987.

Robertson, M., Fukai, S., Hammer, G., and Ludlow, M.: Modelling root growth of grain sorghum using the CERES approach, Field Crop. Res., 33, 113-130, https://doi.org/10.1016/0378-4290(93)90097-7, 1993.

Ryel, R., Caldwell, M., Yoder, C., Or, D., and Leffler, A.: Hydraulic redistribution in a stand of Artemisia tridentata: evaluation of benefits to transpiration assessed with a simulation model, Oecologia, 130, 173-184, https://doi.org/10.1007/s004420100794, 2002.

Schroder, J., Groenwold, J., and Zaharieva, T.: Soil mineral nitrogen availability to young maize plants as related to root length density distribution and fertilizer application method, NJAS-Wagen. J. Life Sci., 44, 209-225, 1996.

Seneviratne, S.I., Corti, T., Davin, E. L., Hirschi, M., Jaeger, E., B., L., I., Orlowsky, B., and Teuling A. J.: Investigating soil moisture-climate interactions in a changing climate: a review, Earth-Sci. Rev, 99, 125–161, https://doi.org/10.1016/j.earscirev.2010.02.004, 2010.

Stöckle, C.O., Donatelli, M., and Nelson, R.: CropSyst, a cropping systems simulation model, Eur. J. Agron., 18, 289-307, https://doi.org/10.1016/s1161-0301(02)00109-0, 2003.

Supit, I., Hooijer, A., and Van Diepen, C.: System description of the WOFOST 6.0 crop simulation model implemented in CGMS, vol. 1: Theory and Algorithms, Joint Research Centre, Commission of the European Communities, EUR 15956, 146, 1994.

Van Dam, J.C.: Field-Scale Water Flow and Solute Transport. SWAP ModelConcepts, Parameter Estimation and Case Studies, Wageningen University, Wageningen, The Netherlands, pp. 167, 2000.

Van der Tol, C., Verhoef, W., Timmermans, J., Verhoef, A., and Su, Z.: An integrated model of soil-canopy spectral radiances, photosynthesis, fluorescence, temperature and energy balance, Biogeosciences, 6, 3109-3129, https://doi.org/10.5194/bg-6-3109-2009, 2009.

Van Genuchten, M.T.: A closed-form equation for predicting the hydraulic conductivity of unsaturated soils, Soil Sci. Soc. Am. J., 44, 892–898, https://doi.org/10.2136/sssaj1980.03615995004400050002x, 1980.

Wang, E. and Smith, C.J.: Modelling the growth and water uptake function of plant root systems: a review, Aust. J. Agr. Res., 55, 501-523, https://doi.org/10.1071/ar03201, 2004.

Wang, Y., Cai, HJ, Yu, LY., Peng XB., Xu JT., and Wang XW.: Evapotranspiration partitioning and crop coefficient of maize in dry semi-humid climate regime, Agric. Water Manage[preprint], 236, https://doi.org/10.1016/j.agwat.2020.106164, 2020.

Wang, Y., Cai, HJ., Zeng, YJ., Su, Z., and Yu, LY.: Data underlying the research on Seasonal and interannual variation in evapotranspiration, energy flux, and Bowen ratio over a dry semi-humid cropland in Northwest China, 4TU. Centre for Research Data. Dataset, https://doi.org/10.4121/uuid:aa0ed483-701e-4ba0-b7b0-674695f5f7a7, 2019.

640 Wang, Y., Zeng, YJ., Yu, LY, Yang P., Van der Tol C., Su, Z., and Cai, HJ.: Integrated Modeling of Photosynthesis and Transfer of Energy, Mass and Momentum (SCOPE_STEMMUS v1.0), Zenodo, https://doi.org/10.5281/zenodo.3839092, 2020.

Wiesler, F. and Horst, W.: Root growth and nitrate utilization of maize cultivars under field conditions, Plant Soil, 163, 267-277, https://doi.org/10.1007/bf00007976, 1994.

645 Williams, J., Jones, C., Kiniry, J., and Spanel, D.A.: The EPIC crop growth model. Transactions of the ASAE, 32, 497-0511, https://doi.org/10.13031/2013.31032, 1989.

Williams, J.R., Gerik, T., Francis, L., Greiner, J., Magre, M., Meinardus, A., Steglich, E., and Taylor, R.: EPIC – Environmental Policy Integrated Climate Model – UsersManual version 0810, Blackland Research and Extension Center – Texas A&MAgriLife, Temple, TX, 2014.

650 Wu, L., McGechan, M., Watson, C., and Baddeley, J.: Developing existing plant root system architecture models to meet future agricultural challenges, Adv. Agron., 85, 85004-85001, https://doi.org/10.1016/s0065-2113(04)85004-1, 2005.

Xu, L. and Baldocchi, D. D.: Seasonal trends in photosynthetic parameters and stomatal conductance of blue oak (Quercus douglasii) under prolonged summer drought and high temperature, Tree Physiol., 23(13), 865-877, https://doi.org/10.1093/treephys/23.13.865, 2003.

655 Yu, L., Zeng, Y., Su, Z., Cai, H., and Zheng, Z.: The effect of different evapotranspiration methods on portraying soil water dynamics and ET partitioning in a semi-arid environment in Northwest China, Hydrol. Earth Syst. Sci., 20, 975-990, https://doi.org/10.5194/hess-20-975-2016, 2016.

Yu, L., Zeng, Y., Wen, J., and Su, Z.: Liquid-Vapor-Air Flow in the Frozen Soil, J. Geophys. Res.-Atmos., 123(14), 7393-7415, https://doi.org/10.1029/2018jd028502, 2018.

660 Zeng, Y., Su, Z., Wan, L., and Wen, J.: A simulation analysis of the advective effect on evaporation using a two-phase heat and mass flow model, Water Resour. Res., 47(10), W10529, https://doi.org/10.1029/2011wr010701, 2011a.

Zeng, Y., Su, Z., Wan, L., and Wen, J.: Numerical analysis of air-water-heat flow in unsaturated soil: Is it necessary to consider airflow in land surface models?, J. Geophys. Res.-Atmos., 116(D20), D20107, https://doi.org/10.1029/2011jd015835, 2011b.

665 Zeng, Y. and Su, Z.: STEMMUS: Simultaneous Transfer of Engery, Mass and Momentum in Unsaturated Soil, University of Twente, Faculty of Geo-Information and Earth Observation (ITC), Enschede, 2013.

https://doi.org/10.5194/gmd-2020-85
Preprint. Discussion started: 2 June 2020


Geoscientific Model Development Discussions

Zheng, Z. and Wang, G.: Modeling the dynamic root water uptake and its hydrological impact at the Reserva Jaru site in Amazonia, J. Geophys. Res.-Biogeosci., 112, https://doi.org/10.1029/2007jg000413, 2007.

Zhou, S., Duursma, R.A., Medlyn, B.E., Kelly, J.W., and Prentice, I.C.: How should we model plant responses to drought? An analysis of stomatal and non-stomatal responses to water stress, Agric. For. Meteorol., 182, 204-214, https://doi.org/10.1016/j.agrformet.2013.05.009, 2013.

Zhou, S., Yu B., Huang Y., and Wang G.: The effect of vapor pressure deficit on water use efficiency at the subdaily time scale, Geophys. Res. Lett., 41, 5005–5013, doi:10.1002/2014GL060741, 2014.

Zhou, S., Yu, B., Zhang, Y., Huang, Y., and Wang, G.: Partitioning evapotranspiration based on the concept of underlying water use efficiency, Water Resour. Res., 52, 1160-1175, https://doi.org/10.1002/2015wr017766, 2016.

Zhu, S., Chen, H., Zhang, X., Wei, N., Shangguan, W., Yuan, H., Zhang, S., Wang, L., Zhou, L., and Dai, Y. Incorporating root hydraulic redistribution and compensatory water uptake in the Common Land Model: Effects on site level and global land modeling, J. Geophys. Res.-Atmos., 122, 7308-7322, https://doi.org/10.1002/2016jd025744, 2017.

Zhuang, J., Nakayama, K., Yu, G.-R., and Urushisaki, T.: Estimation of root water uptake of maize: an ecophysiological perspective, Field Crop. Res., 69, 201-213, https://doi.org/10.1016/s0378-4290(00)00142-8, 2001a.

Zhuang, J., Yu, G., and Nakayama, K.: Scaling of root length density of maize in the field profile, Plant Soil, 235, 135-142, https://doi.org/10.1023/A:1011972019617, 2001b.